NETWORKS AND HETEROGENEOUS MEDIA
©American Institute of Mathematical Sciences
Volume **1**, Number **3**, September **2006**

Website: http://aimSciences.org

pp. **399–439**

MATHEMATICAL MODELLING OF CANCER INVASION OF TISSUE: DYNAMIC HETEROGENEITY

M.A.J Chaplain and G. Lolas

The SIMBIOS Centre, Division of Mathematics
University of Dundee, Dundee DD1 4HN

(Communicated by Luigi Preziosi)

Abstract. Solid tumours grow through two distinct phases: the avascular and the vascular phase. During the avascular growth phase, the size of the solid tumour is restricted largely by a diffusion-limited nutrient supply and the solid tumour remains localised and grows to a maximum of a few millimetres in diameter. However, during the vascular growth stage the process of cancer invasion of peritumoral tissue can and does take place. A crucial component of tissue invasion is the over-expression by the cancer cells of proteolytic enzyme activity, such as the urokinase-type plasminogen activator (uPA) and matrix metalloproteinases (MMPs). uPA itself initiates the activation of an enzymatic cascade that primarily involves the activation of plasminogen and subsequently its matrix degrading protein plasmin. Degradation of the matrix then enables the cancer cells to migrate through the tissue and subsequently to spread to secondary sites in the body.

In this paper we consider a relatively simple mathematical model of cancer cell invasion of tissue (extracellular matrix) which focuses on the role of a generic matrix degrading enzyme such as uPA. The model consists of a system of reaction-diffusion-taxis partial differential equations describing the interactions between cancer cells, the matrix degrading enzyme and the host tissue. The results obtained from numerical computations carried out on the model equations produce dynamic, heterogeneous spatio-temporal solutions and demonstrate the ability of a rather simple model to produce complicated dynamics, all of which are associated with tumour heterogeneity and cancer cell progression and invasion.

1. **Introduction.** The word cancer is an "umbrella term" for approximately 200 diseases. There are two broad categories of tumours: Benign and Malignant ([2]). Benign tumours remain localized to the tissue in which they arise and although they may grow large, they will not spread to other parts of the body. Commonly, they are completely enclosed in a protective capsule of collagenous tissue and they typically do not prove fatal unlike malignant tumours. If found early, benign tumours can be cured either by surgical removal or in some cases by radiation therapy. Unlike benign tumours, and even though both benign and malignant tumours grow in an uncontrolled way, malignant ("cancerous") tumours are a far more serious matter. Some of their cells break off from the main primary tumour mass, invading and destroying surrounding tissue or travelling through the blood or lymph system to

2000 *Mathematics Subject Classification.* Primary: 58F15, 58F17; Secondary: 53C35.

Key words and phrases. cancer invasion of tissue, matrix degrading enzyme, chemotaxis, haptotaxis, spatio-temporal heterogeneity.

distant parts of the body, where new tumours might form. These malignant cells could break off again and establish even more colonies ([46]).

At the early growth stage the tumour is relatively harmless and is still *avascular*, that is, it lacks its own network of blood vessels for supplying nutrients, including oxygen, and for removing wastes ([41],[42]). The critical event that converts a self-contained pocket of aberrant cells into a rapidly growing malignancy comes when the tumour becomes *vascularized* ([42]).

Cancers also possess the ability to actively invade the local tissue and then spread throughout the body. Invasion and metastasis are the most insidious and life-threatening aspects of cancer ([57], [58]). Whether physiological or malignant invasion, the regulation for its necessary events involves spatial and temporal co-ordination, as well as certain cyclic "on-off" processes, at the level of individual cells. Motility, coupled with regulated, intermittent adhesion to the extracellular matrix and degradation of matrix molecules, allows an invading cell to move through the three-dimensional tissue matrix. At the leading edge of the motile cell, receptor-ligand and proteolytic-antiproteolytic complexes coordinate sensing, protrusion, burrowing and traction of the cell ([58], [55]).

The most significant turning point in the disease (cancer), however, is the establishment of metastasis. Metastasis is defined as the formation of secondary tumour foci at a site discontinuous from the primary tumour ([57], [58]). Metastasis unequivocally signifies that a tumour is malignant and this is in fact what makes cancer so lethal. In principal, metastases can form following invasion and penetration into adjacent tissues followed by dissemination of cells in the blood vascular system (hematogeneous metastasis) and lymphatics (lymphatic metastases) [3]. The molecular mechanisms of metastasis are poorly understood as a result of their apparent complexity. However, sequential steps in the so-called "*metastatic cascade*" are believed to include the following:

- metastatic cells arise within a population of neoplastic/tumourigenic cells as a result of genomic instabilities;
- vascularization of the tumour through the angiogenesis process;
- detachment of metastatic-competent cells that have already evolved;
- migration of the metastatic cells;
- local invasion of cancer cells into the surrounding tissue, requiring adhesion to and subsequent degradation of extracellular matrix (ECM) components;
- transport of metastatic cells either travelling individually or as emboli composed of tumour cells (homotypic) or of tumour cells and host cells (heterotypic);
- metastatic cells survive their journey in the circulation system;
- adhesion/arrest of the metastatic cells at the secondary site, cells or emboli arrest either because of physical limitations (i.e. too large to traverse a lumen) or by binding to specific molecules in particular organs or tissues;
- escape from the blood circulation (extravasation);
- proliferation of the metastatic tumour cells;
- growth of the secondary tumour in the new organ.

Metastases can appear shortly after surgery but can also remain undetected for more than a decade before manifesting themselves clinically ([19], [40]). This indicates that disseminated cancer cells can persist in a dormant state, unable to form a progressively increasing tumor mass ([19]) Such heterogeneity of outcome indicates that the fate of tumour cells that disseminate to distant organs before

surgery must be regulated by either inherent cancer cell properties or the milieu of the target organs, or both. Identifying the mechanisms that keep metastases in their dormant, occult state is one of the most challenging and important avenues of cancer research ([19], [40]).

In this paper we present a mathematical model for invasion of tissue by cancerous cells, focussing on the role of matrix degrading enzymes, chemotaxis and haptotaxis. This initial model is a simplification of that presented in [23] and enables one to focus on the potential competition between chemotaxis and haptotaxis. In a development of this basic model, the inclusion of a nonlinear haptotaxis function demonstrates the ability of this simple model to produce dynamic, heterogeneous solutions. Next, through the incorporation of limit-cycle kinetics into the proliferation terms of the model (representing the observed cycles in uPA receptor dynamics and endocytosis) we observe the effect this has on the spatio-temporal behaviour of the solutions. Finally, we present two-dimensional computational simulations of the full model developed by Chaplain and Lolas [23].

In the next two sections, we present a brief overview of the underlying biology of extracellular matrix degradation and cell migration, before developing the mathematical model in section 4. In section 5 we present the results of computational simulations of our model and conclude the paper with a discussion section.

2. **Proteolysis and extracellular matrix degradation.**

The prognosis of a cancer is primarily dependent on its ability to invade and metastasize. Many steps that occur during tumour invasion and metastasis require the regulated turnover of extracellular matrix (ECM) macromolecules. Breakdown of the ECM is accomplished by the concerted action of two general classes of proteases: the metalloproteinases and the serine proteases ([6], [7]).

However, proteolytic degradation of the extracellular matrix is essential for the processes of tissue remodelling as well. These processes take place in a number of distinct physiological events in the healthy organism, such as trophoblast invasion, mammary gland involution, and skin wound healing. The plasminogen activation system has an important position among the extracellular proteases engaged in these degradation reactions. This system is organized as a proteolytic cascade with active proteases and their pro-enzymes, protease inhibitors, and extracellular binding proteins. In the following section, we will demonstrate the pleiotropic activities that the urokinase plasminogen activation system has in cell migration, cell movement, tumour progression, and metastasis ([13], [6], [7]).

2.1. **Structure and function of the plasminogen activation system.**

The enzymatic system consists of the urokinase receptor (uPAR), urokinase plasminogen activator (uPA), the matrix-like protein vitronectin (VN) and plasminogen activator inhibitors: type-1 (PAI-1) and type-2 (PAI-2). uPA is an extracellular serine protease produced from cells as a single-chain proenzyme pro-uPA. Two major functional domains make up the uPA molecule: the protease domain and the growth factor domain. The protease moiety activates plasminogen and, hence, generates plasmin, a serine protease capable of digesting basement membrane and extracellular matrix proteins. Thus, the unrestrained generation of plasmin from plasminogen by the action of plasminogen activator (PA) is potentially hazardous to cells. In this regard, the process of plasminogen activation in a healthy organism is strictly controlled through the availability of PAs, localized activation, and interaction with specific inhibitors (PAIs). One of these inhibitors, PAI-1, which is believed to be

the most abundant, fast-acting inhibitor of uPA *in vivo* ([6], [7]). In other words, for cells to protect themselves they must secrete a surplus of inhibitors to guarantee restraint of pericellular proteolysis. Indeed secreted uPA is often associated with plasminogen activator inhibitor-1 (PAI-1) and remains inactive.

The growth factor domain has no protease activity but can bind a specific, high affinity cell-surface receptor, uPAR (or CD87). uPAR is expressed in considerable amounts on the cell surface of various cell types such blood leukocytes, endothelial cells, macrophages, fibroblasts, and by different types of cells in human cancer. In addition, as implied by its name, uPAR was first identified as a high-affinity receptor for uPA. uPAR mediates the binding of the zymogen pro-uPA to the plasma membrane where plasmin converts pro-uPA to the active zymogen, uPA, which in turn converts plasma membrane-associated plasminogen into plasmin ([6], [7]). Importantly, uPA is not the only ligand for uPAR that is able to bind to the matrix-like form of vitronectin (VN) and thus place emphasis on a non-proteolytic role for uPAR ([81], [24]). uPAR contains a vitronectin binding site(s) distinct form the urokinase binding site. The strength of interaction between uPAR and VN is not mutually exclusive; rather inactive pro-uPA, as well as active uPA promote VN binding. In addition, uPAR can also bind integrins at sites distinct from its uPA- and VN-binding sites. These interactions account for the effects of uPAR on cell adhesion and migration ([83]).

Vitronectin is a versatile glycoprotein that is found in circulation, in the extracellular matrix of endothelial cells, and within various tissues of the human body ([26]). As the name indicates, VN binds strongly to glass surfaces (*vitro* = glass). Interactions with an assortment of biological molecules are responsible for the multiple functions exhibited by vitronectin. Other functions of the protein that are confined to surfaces or tissues include cell-adhesion and regulation of pericellular proteolysis ([26]). Moreover VN functions as the major high-affinity binding protein of PAI-1, uPAR and integrins. Since VN is recognized as the major binding protein of PAI-1, and its binding to uPAR could be expected to bring PAI-1 in close approximation with uPA, thereby promoting inhibition and clearance of uPA from its receptor uPAR. We postulate that this process may effect a lower avidity of cellular attachment to vitronectin. In this paradigm, PAI-1, although decreasing uPA activity, would also promote detachment of the cell from its contact site. Thus, PAI-1 in circumstances where sustained proteolytic activity is not vital to movement could *promote* rather than retard migration.

PAI-1, the inhibitor of uPA, belongs to the serpin (**ser**ine **p**rotein **in**hibitors) family ([6], [7]) and can specifically bind to and inhibit not only free, but also receptor-bound uPA. When PAI-1 is available, it can bind to the uPA/uPAR complex triggering the internalization of the uPA/uPAR/PAI-1 complex by receptor-mediated endocytosis. The uPA/uPAR/PAI-1 complex will be dissociated and PAI-1 and uPA will be digested, but the receptor will be recycled to the cell surface and concentrate the uPA (if available) on the cell surface again. This process will lead to clearing of PAI-1 from the vicinity of the cell surface ([27], [28], [65]). It is not clear why PAI-1 is concentrated in the nucleus of the cancer cell. However, many receptor-binding proteins bind to the receptor and are then endocytosed. It is, therefore, conceivable that such protein signalling (or their degradation products) acts directly within the cell, or cell nucleus. It has been reported that the receptor-mediated internalization of uPA/uPAR/PAI-1 complexes may trigger the proliferation of the cancer cells. Additionally, inhibition of cell adhesion and migration by PAI-1 on VN occurs

because the same region of VN is required for interaction with PAI-1, uPAR and integrins. In other words, PAI-1 competes with uPAR for binding to VN.

The uPA/uPAR/PAI-1/VN system therefore appears to be a very important function in the regulation of the attachment/detachment machinery, namely to inform cells when, how and where to move. Availiable data suggests that cells respond to a "go" signal through the stimulation of surface proteolysis, exposure to chemotactic epitope(s), and recycling of "naked" uPAR to novel surface proteolysis, and to a "stop" signal via PAI-1-dependent internalization and degradation of uPA. Additionally, cells respond to a "pause" signal through transient uPAR-dependent adhesion stages, thus shifting the cells between an "adhesion - mode" and a "migration - mode". Thus occupation of cell surface uPAR by uPA and concomitant urokinase activity are ephemeral in the settings of this protease inhibitor.

3. **Proteolytic stimulation of cell migration.** Cell migration plays a central role in a wide variety of physiological and pathophysiological processes, for instance embryonal development, inflammation, and cancer metastasis (for reviews see [55]). Cell migration is the locomotion of a cell on a substratum of ECM proteins. Cells require attachment sites on extracellular matrices in order to reorganize their cytoskeleton and initiate protrusions important to migration. In this regard, cancer cells require a well-regulated, pericellular proteolysis to migrate.

Cell migration proceeds through extension of the leading cytoplasmic edge, a process which among other events involves adhesion, mediated by several proteases and their extracellular matrix protein ligands. Such interactions lead to the generation of specific intracellular signals and reorganization of the cytoskeleton. The adhesions at the leading cellular edge are thought to provide guidance and traction for pulling the cell body forward. Dissociation of integrin/ligand and cell surface receptor/ligand complexes, via regulated signals delivered from the cell interior, allows retraction of the trailing edge ([55]).

This adhesion may not be so stringent as to prevent movement, nor too weak to provide traction. The extent of migration may thus vary with the avidity of adhesion. In addition, adhesion must be regulatable or reversible to allow detachment. Extracellular proteolytic enzyme systems like the plasminogen activation system may facilitate release of the trailing edge by degradation of ECM proteins. Several proteases are involved in cell migration and invasion, but an important role has been ascribed to the plasminogen activation system.

The effects of the plasminogen activation system in cell migration may be due to a proteolytic as well as a non-proteolytic mechanism ([6], [7]). A proteolytic mechanism of cell migration implies plasmin generation at focal adhesion sites, catalyzed by uPAR-bound uPA, which could help to break physical barriers and promote detachment of the trailing edge of the cells from matrix proteins that might impede their migration. On the other hand, with a non-proteolytic mechanism, uPA is thought to promote cell migration by enhancing adhesion at the leading edge, through stimulation of binding of uPAR to VN, modulation of uPAR/integrin interactions and/or by initiation of signal transduction cascades ([83]). It is also possible that both mechanisms operate simultaneously in migrating cells.

Soon after it was reported that uPAR contains a vitronectin-binding site, it was realized that active PAI-1 blocks the interaction of uPAR and vitronectin. In this regard, Waltz *et al.* (1997) and Deng *et al.* ([34]) reported that PAI-1 regulates proteolytic activity (both on the cell surface and in solution), blocks binding of and

adhesion to vitronectin by myeloid cells and also blocks binding of soluble uPAR (suPAR)-that is lacking the GPI-anchor- to vitronectin. Moreover in [48], Kanse *et al.* ([48]) demonstrated that PAI-1 blocks binding of vitronectin to uPAR on endothelial cells. Inhibition of both uPA activity and of uPA/uPAR interactions prevents extracellular matrix degradation. On the other hand, when PAI-1 binds to VN, it interferes with vitronectin recognition by integrins, thereby stimulating release of cells from the matrix and paradoxically *supporting* cell migration.

It seems possible to arrive at a model unifying the many observations by assuming that proteolytic and non-proteolytic mechanisms of uPA action on cell migration are operating simultaneously in individual migrating cells. If pro-uPA is converted to active uPA at the ventral surface of the cells, non-proteolytic mechanisms could dominate at the leading edge and proteolytic mechanisms at the trailing edge. The relative importance of the proteolytic and the non-proteolytic elements and the net effect of (pro-)uPA and PAI-1 would be expected to depend on the level of expression by the migrating cells of uPAR, endocytosis receptors, and integrins, of the composition of the ECM, of the pericellular localization of (pro-)uPA and PAI-1, of mechanisms for pro-uPA activation, and of the stimuli that induce cell motility.

3.1. **Chemotaxis and haptotaxis.** Tumour cells encounter a variety of soluble and substratum-bound factors which may influence their directed migration at different stages in the process of tumour invasion and metastasis. Such factors can promote the directed movement of tumour cells by at least two mechanisms, termed chemotaxis and haptotaxis.

Chemotaxis is defined as cellular locomotion directed in response to a concentration gradient of a chemical factor in solution ([53]). Cells sense the chemical and migrate toward higher concentrations of this substance until they reach the source secreting it. On the other hand, gradients do not have to be in solution. An adhesive molecule could be present in increasing amounts along an extracellular matrix. A cell that was constantly making and breaking adhesions with such a molecule would move from a region of low concentration to an area where that adhesive molecule was more highly concentrated. Such a phenomenon is called **haptotaxis** ([17], [29]).

The potential importance of a chemotactic response to ECM components is apparent when considering that during the process of tumour invasion and metastasis, proteolytic degradation results in solubilization of ECM components ([56], [9]). As a result, tumour cells could conceivably detect and respond to the soluble fragments as well as to the insoluble intact matrix molecules. Therefore, chemotaxis and haptotaxis to ECM components represent two separate and distinguishable means by which tumour cells penetrate membranes and interstitial stroma ([56], [9]).

Induction of chemotaxis and chemokinesis by uPA has been reported in a variety of cell types ([67], [45], [74], [38]). This activity is exerted through its specific, high affinity cell surface receptor uPAR (or CD87) ([45], [74]). The receptor anchors uPA at the leading edge of migrating cells and localizes it at the focal contacts and to cell-to-cell contact sites ([13], [12], [38]). These sites also contain adhesion molecules, integrins, cadherins, cytoskeleton-connecting proteins, and signal transducing molecules.

Cell motility (e.g. chemotaxis, chemokinesis, migration) stimulated by active uPA can involve plasmin generation and the subsequent degradation of ECM proteins and/or proteolytic trimming of cell surface components, including adhesion

receptors and uPAR itself. uPAR has been reported to associate with many signaling molecules and to mediate signal transduction ([83], [1], [84]). Much attention has been focused on the possibility that uPA binding uPAR activates intracellular signal transduction cascades. Recent reports observed that the binding of uPA to uPAR in tumour or endothelial cells activates the mitogen-activated protein kinases extracellular regulated kinase 1 and 2 (ERK-1, ERK-2) ([64]). However, a major question is how uPAR mediates cellular signaling, since uPAR is not a transmembrane molecule but belongs to the group of proteins that are tethered to the plasma membrane.

The membrane attachment of uPAR via a GPI anchor, *i.e.* the lack of an intracytoplasmic region capable of connecting with the cytoplasmic signal transducers, suggests the existence of one or more hypothetical "transmembrane adapter molecules" that connects uPAR and signalling molecules ([6], [7]). Integrins may serve as such signal transducers, and indeed uPAR has been shown to be associated in the plasma membrane with complexes of integrins and tyrosin kinases suggesting a role for these complexes in transmembrane transmission of signals via uPAR. uPA/uPAR interaction causes catalytically independent responses in endothelial cells, including chemotaxis and chemokinesis. Based on the fact that the binding of ligands to integrins initiates a signal-transduction cascade it was speculated that the reported binding of uPA to the ligand VN is involved in initiation of a signal transducing cascade ([6], [7]).

Certain actions of uPA on different cell types in culture suggest that a signal is initiated by binding of uPA to uPAR. A chemotactic activity of uPA has long been recognized in vitro on different cell types in culture ([15], [45], [74]). The chemotactic activity of uPA strictly depends on binding to its receptor uPAR: it does not occur in murine cells lacking uPAR, or containing uPAR but not recognizing human uPA; it can be restored by transfection of the uPAR; and it is inhibited by antibodies that prevent uPA/uPAR interaction ([74]). Occupancy of uPAR transduces a signal that results in the movement of cells; indeed uPA binding to uPAR activates several tyrosine kinases ([15], [74]). It is noteworthy that the signaling pathways activated by uPA/uPAR seem to be the same pathways that induce their own expression. Thus, it is possible that over-expression of the uPA/uPAR system in tumour cells leads to a signalling loop and/or activation of additional mechanisms dependent on these molecules that contribute to enhanced pericellular proteolysis, migration and proliferation ([1]).

3.2. **Cell adhesion and haptotaxis.** Both cell-cell interactions and cell-stroma interactions play an important role during the invasive cascade. Connections through cell adhesion molecules, integrins, and cadherins stabilize tissue integrity, whereas loss or alteration of these cell surface proteins has been shown to be associated with increased metastatic potential. The strength and duration of cellular interactions are modulated by (a) the repertoire of receptor expression (especially integrins); (b) the relative abundance of adhesive and counteradhesive factors in the extracellular matrix; and (c) extracellular hydrolytic enzyme systems. In this regard, pericellular proteolysis initiated by the plasminogen activator/plasmin system fulfils pivotal functions in cellular migration. Direct binding of plasminogen activators and plasminogen/plasmin to cell surface receptors or to extracellular matrix drastically increases the local concentration and the efficiency of protease formation/action. The nonclassical activities of the plasminogen activation system and the pericellular cooperation of its components with adhesion receptors, extracellular matrix

(ECM) proteins and signalling molecules, have provided new insights into their role as molecular coordinators of cell adhesion.

The classical role of plasminogen activation is one counteracting cell-substratum and cell-cell adhesion, as pericellular plasmin generation leads to degradation of adhesion receptors and their extracellular matrix ligands ([61]). However, under some conditions, binding of uPA to uPAR promotes cell-substratum adhesion. In this regard, binding of uPA to uPAR stimulates the adhesion of several integrin-independent cell lines to VN. On the other hand, PAI-1 inhibits uPAR-dependent adhesion to VN. These observations show that uPA and uPAR may also affect cell adhesion. Additionally, the avidity of uPAR for VN is strongly promoted by occupancy of the receptor with uPA.

Recently, it has become clear that uPAR is involved in cell-stroma interactions and signal transducing events that are independent of its role in plasminogen activation. Both the expression pattern of uPAR and its proximity to adhesion and signalling molecules places this protease receptor at the crossroads of cellular adhesion. uPAR can be found at various locations depending on the cell type and activation state ([50]). For example, it can be found at the apical surface of quiescent epithelial or endothelial cells or concentrated at focal or cell-cell contacts in invasive cells in association with other proteins, such as ECM adhesion molecules, cytoskeletal elements, integrins and signalling factors. It participates in cell adhesion directly by binding to vitronectin and indirectly by modulating the affinity of integrins for their complementary ligands ([71]).

uPAR has been shown to bind not only uPA, but also but also the extracellular matrix protein, vitronectin (VN). By virtue of the latter activity, it acts as an adhesion receptor ([83]). The vitronectin/uPAR complex is enhanced by the simultaneous binding of urokinase ([83], [48]). The uPA/uPAR interaction increases the binding of vitronectin to the cells meaning that, somewhat paradoxically, uPA promotes cell adhesion. In this regard, it has been proposed by Wei *et al.* ([83]) that the interaction of uPAR binding to vitronectin takes part in a balanced attachment and release scenario, directed by the PAI-1, which competes with uPAR in the vitronectin binding process ([34]).

A further, indirect role of uPAR in adhesion is provided by interactions with certain integrins, influencing the binding properties of the latter ([83], [80]). This broadens the currently held concept of uPAR-integrin interactions, in which uPAR is proposed to interact exclusively with integrins residing on the same cell (cis interaction) as an "associated protein" that mediates signal transduction directly or through the mediation of a distinct transmembrane adaptor protein. The simultaneous recognition of vitronectin by uPAR and integrins co-localizes these two receptors to adhesion structures and directs (haptotaxis) the proteolytic activity of plasminogen systems to the matrix.

Likewise, to make matters even more complicated, active PAI-1, which is the main PA antagonist, serves as a potent competitor for vitronectin binding to uPAR and integrins and thus disrupts uPAR-mediated adhesion, but also sterically inhibits integrin binding to vitronectin. Vitronectin is considered the primary PAI-1 binding plasma protein. Like PAI-1, vitronectin is significantly increased at sites of disease, or injury, where it binds collagens, uPAR or integrins. PAI-1 also seems to play a central role in cell adhesion mediated through integrins or the uPA/uPAR complex. However, when PAI-1 inhibits uPA or when PAI-1 binds vitronectin, the uPA/uPAR complex no longer interacts with vitronectin. The higher affinity of

PAI-1 to vitronectin than that of the uPA/uPAR complex to vitronectin is likely to be responsible for the release of cells from this substratum by an excess of PAI-1 (Czekay *et al.*, 2003). Therefore Deng *et al.* ([34]) suggested that the delicate balance between cell adhesion and cell detachment is governed by PAI-1. It is tempting to speculate that the de-adhesive effects of PAI-1 are related to the observation that high PAI-1 levels are associated with a poor prognosis for survival in several metastatic human cancers ([7]).

4. **Spatio-Temporal models of the uPA system and tissue invasion.** In this section evolution equations (partial differential equations) describing the "kinesis", "taxis" and reactions of the urokinase plasminogen activation system (consisting of cancer cells, urokinase plasminogen activator (uPA) and extracellular matrix components *i.e.* vitronectin, fibronectin, laminin) are derived and developed to consider several key components of the system. In this regard, the components of this chapter are arranged as follows. First, we look at previous attempts to investigate tumour invasion and metastasis using deterministic continuum models. We will then discuss the basic framework of the urokinase plasminogen activation system and also discuss the estimation of various parameters of the model that can be obtained using experimental results whenever this is possible. We then present simulation results of the model.

Previously several studies have incorporated mathematical models for cancer invasion and metastasis e.g. [21], [44], [66], [16], [69], [70], [4], [5], [23]. Many of these papers examine how cancer cells respond to ECM gradients via haptotaxis. The gradients are created through the degradation of the ECM by matrix degrading enzymes (MDEs). In this paper, we will base our initial mathematical model on generic solid tumour growth, which for simplicity we assume is at the avascular stage, focusing solely on the interactions between the cancer cells and the surrounding tissue. We initially develop a mathematical model consisting of three coupled partial differential equations (PDEs) describing the evolution in time and space of the system variables. The key physical variables are assumed to be the tumour cell density (denoted by c); extracellular matrix protein density (denoted by v) and the urokinase plasminogen activator concentration (denoted by u).

We now describe the way in which the tumour cell density $c(x,t)$, the urokinase plasminogen activator (uPA) protease concentration $u(x,t)$ and the extracellular matrix density $v(x,t)$ are involved in invasion and derive partial differential equations governing the evolution of each variable.

(a) ***Cancer cells:***

We assume that there is a change in cell number density due to dispersion, arising from random locomotion and we take D_c as the cell random motility coefficient, characterising how cells would disperse from higher to lower densities. However, in some cases we will use a physically meaningful expression to describe their random motion other than the common linear diffusion and therefore nonlinear diffusion will be also used. We assume that $D \propto D(c^p, v^q, u^r), (p,q,r \geq 1)$; for example the case $D(c,v,u) = u\,v$ is a representative example illustrating a chemokinetic response *i.e.* increased random dispersion will be observed for regions of high uPA and VN concentrations.

In addition, the important features that the nonlinearity of the random motility captures are the finite speed of dispersion as well as the preservation of initial conditions of compact support. In other words, this means that if the initial cancer

cell profile is localized in a finite region then at all subsequent times it will be confined to a finite region whose size however could change over time. On the other hand by choosing D_c to be constant we impose that an infinitesimally small density of cancer cells penetrate the entire spatial domain immediately which is physically unrealistic. However such a choice does not affect the general framework of the process since the contribution of the chemokinetic term D_c is always the smallest in cancer cell locomotion.

The second most important term that quantifies the change in cell number density is that of the "*directional flow*" of cells due to spatial gradients of environmental stimuli, such as those stimulating chemotactic or haptotactic responses. We refer to this directed movement of tumour cells in the urokinase plasminogen activation model as chemotaxis and haptotaxis - namely a response to gradients of diffusible and non-diffusible macromolecules such as urokinase plasminogen activator ([12], [38], [13]) and vitronectin ([9]) respectively. To incorporate this response into our mathematical model we take the cancer cell flux (due to gradients) to be $\mathbf{J_{flux}} = \mathbf{J_{chemo}} + \mathbf{J_{hapto}}$, namely $\mathbf{J_{flux}} = \chi_c c\nabla u + \xi_c c\nabla v$, where $\chi_c, \xi_c > 0$ are the chemotactic and haptotactic coefficients respectively, characterising biased directional movement in response to spatial gradients.

Regarding the proliferation of cancer cells, we assume that in the absence of any extracellular matrix (ECM), cancer cell proliferation satisfies a logistic growth law. The presence of ECM leads to competition for space between the cancer cells and the ECM and we model this by including a crowding term which is proportional to the product cv. This distinguishes our model from the one proposed by Anderson *et al.* ([4]) since they do not consider any cell proliferation in order for them to focus entirely on cell-matrix interactions. On the contrary, Byrne *et al.* [16] consider a similar term in their work concerning trophoblast invasion.

To summarise, the conservation of mass applied to the cancer cell density c leads to the following equation:

$$\frac{\partial c}{\partial t} + \nabla \cdot (\mathbf{J_{random}} + \mathbf{J_{chemotaxis}} + \mathbf{J_{haptotaxis}}) \;=\; R_c \,,$$

where R_c is the net rate of production or loss of cells by mechanisms other than migration (*e.g.* proliferation or death) and hence the resulting partial differential equation for the cancer cell motion is,

$$\frac{\partial c}{\partial t} = \underbrace{\nabla \cdot (D_c \nabla c)}_{\text{dispersion}} - \underbrace{\nabla \cdot (\chi_c c \nabla u)}_{chemotaxis} - \underbrace{\nabla \cdot (\xi_c c \nabla v)}_{haptotaxis} + \underbrace{\mu_1 \; c \; (1 - \frac{c}{c_o} - \frac{v}{v_o})}_{proliferation} \,, \qquad (1)$$

where D_c is (linear or nonlinear) the random motility coefficient; χ_c and ξ_c are the chemotactic and haptotactic functions respectively. Furthermore, μ_1 is the proliferation rate of the cells, while c_o and v_o are the maximum sustainable tumour cell and extracellular matrix densities respectively.

(b) ***Extracellular matrix***

We now turn attention to the ECM. This is known to contain many macromolecules such as vitronectin, laminin and fibronectin which can be degraded by several matrix degrading enzymes and especially by plasminogen activation. Since ECM is "static", we neglect any random motion and focus solely on its degradation by the uPA protease. We assume that uPA degrades the ECM upon contact and we also suggest that ECM components re-establish or re-model while they are competing for space with the invasive cells in a manner similar to that describing cancer cell

proliferation. Thus, in the absence of cancer cells, extracellular matrix remodels in a logistic manner. On the other hand, the presence of cancer cells leads to competition for space betweeen the cancer cells and the ECM which again we model by incorporating a crowding term into the logistic growth. Using a modified logistic growth with rate constant μ_2 to describe the ECM production, and taking δuv to represent the rate of degradation, we have the following equation for the extracellular matrix:

$$\frac{\partial v}{\partial t} = \underbrace{-\delta\, u\, v}_{proteolysis} + \underbrace{\mu_2\, v\,(1 - \frac{c}{c_o} - \frac{v}{v_o})}_{re-establishment} . \tag{2}$$

[In general $\mu_1 \neq \mu_2$].

(c) ***urokinase Plasminogen Activator (uPA) protease***

Factors influencing the protease concentration are assumed to be diffusion, protease production and protease decay. Specifically, uPA is produced by cancer cells, diffuses throughout the extracellular matrix, with constant diffusion coefficient D_u, and undergoes decay of the form $\beta\, u$. The equation governing the evolution of uPA concentration is therefore given by:

$$\frac{\partial u}{\partial t} = \underbrace{D_u \nabla^2 u}_{dispersion} + \underbrace{\alpha\, c}_{production} - \underbrace{(\beta\, u)}_{decay} . \tag{3}$$

Hence, the complete system of equations describing the interactions between the tumour cells, extracellular matrix and uPA is:

$$\begin{aligned}
\frac{\partial c}{\partial t} &= \underbrace{\nabla\cdot(D_c \nabla c)}_{\text{dispersion}} - \underbrace{\nabla\cdot(\chi_c c \nabla u)}_{chemotaxis} - \underbrace{\nabla\cdot(\xi_c c \nabla v)}_{haptotaxis} + \underbrace{\mu_1\, c\,(1 - \frac{c}{c_o} - \frac{v}{v_o})}_{proliferation} , \\
\frac{\partial v}{\partial t} &= \underbrace{-\delta\, u\, v}_{proteolysis} + \underbrace{\mu_2\, v\,(1 - \frac{c}{c_o} - \frac{v}{v_o})}_{re-establishment} , \\
\frac{\partial u}{\partial t} &= \underbrace{D_u \nabla^2 u}_{dispersion} + \underbrace{\alpha\, c}_{production} - \underbrace{(\beta\, u)}_{decay}
\end{aligned} \tag{4}$$

(d) **Nondimensionalization**

In order to solve the system numerically, we first of all non-dimensionalise the equations. The variables and parameters in the uPA system equations and their associated boundary conditions are transformed into dimensionless quantities using the following reference variables:

1. Reference length scale, L, (*e.g.* the maximum invasion distance of the cancer cells at this early stage of invasion $0.1 - 1cm$),
2. reference time unit, $\tau = \frac{L^2}{D}$, where D is a reference chemical diffusion coefficient *e.g.* $10^{-6} cm^2 s^{-1}$ ([14]). Therefore, we deduce that τ varies between $10^4 - 10^6 sec$.
3. reference tumour cell density c_o, extracellular matrix density v_o and reference uPA concentration u_o (where c_o, v_o and u_o are appropriate reference variables).

We thus define the non-dimensional variables:

$$\tilde{t} = \frac{t}{\tau}, \tilde{x} = \frac{x}{L}, \tilde{c} = \frac{c}{c_o}, \tilde{v} = \frac{v}{v_o}, \tilde{u} = \frac{u}{u_o}.$$

and new parameters via the following scaling:

$$\tilde{D}_c = \frac{D_c}{D}, \tilde{D}_u = \frac{D_u}{D}, \tilde{\chi} = \chi_c \frac{u_o}{D}, \tilde{\xi} = \xi_c \frac{v_o}{D},$$
$$\tilde{\mu}_1 = \mu_1 \tau, \tilde{\mu}_2 = \mu_2 \tau, \tilde{\delta} = \delta u_o \tau, \tilde{\alpha} = \alpha \tau \frac{c_o}{u_o}, \tilde{\beta} = \beta \tau.$$

Henceforth, we omit the tildes for notational simplicity. The dimensionless governing equations can then be written in the following general form:

$$\begin{aligned}
\frac{\partial c}{\partial t} &= \underbrace{\nabla \cdot (D_c \nabla c)}_{\text{dispersion}} - \underbrace{\nabla \cdot (\chi_c c \nabla u)}_{chemotaxis} - \underbrace{\nabla \cdot (\xi_c c \nabla v)}_{haptotaxis} + \underbrace{\mu_1\, c\, (1 - c - v)}_{proliferation}, \\
\frac{\partial v}{\partial t} &= \underbrace{-\delta\, u\, v}_{proteolysis} + \underbrace{\mu_2\, v\, (1 - c - v)}_{re-establishment}, \qquad (5) \\
\frac{\partial u}{\partial t} &= \underbrace{D_u \nabla^2 u}_{dispersion} + \underbrace{\alpha\, c}_{production} - \underbrace{(\beta\, u)}_{decay}.
\end{aligned}$$

(e) ***Boundary and initial conditions.***

In order to close the system, boundary and initial conditions for c, u and v are required.

Boundary conditions: Guided by the *in vitro* experimental protocol in which invasion takes place within an isolated system, we assume that there is no-flux of tumour cells or protease across the boundary of the domain, namely $x = 0$ and $x = 1$, in one-space dimension. These boundary conditions are represented by the following equations,

$$(-D_c \frac{\partial c}{\partial x} + c\, \chi \frac{\partial u}{\partial x} + c\, \xi \frac{\partial v}{\partial x}) = 0, \text{ at } x = 0,\, 1, \qquad (6)$$

$$\frac{\partial u}{\partial x} = 0, \text{ at } x = 0,\, 1. \qquad (7)$$

Initial conditions: Finally, the initial distribution of the tumour cells, the protease concentration and the ECM density are prescribed by the system of equations (8). Initially we assume that there is a cluster of cancer cells already present and that they have penetrated a short distance into the extracellular matrix while the remaining space is occupied by the matrix alone. Finally, for the uPA protease initial concentration we suppose that it is proportional to the initial tumour density. Combining the above we have,

$$\begin{aligned}
c(x,0) &= exp(\frac{-x^2}{\epsilon}),\ x \in [0,1] \text{ and } \epsilon > 0, \\
v(x,0) &= 1 - \frac{1}{2}\, exp(\frac{-x^2}{\epsilon}),\ x \in [0,1] \text{ and } \epsilon > 0, \qquad (8) \\
u(x,0) &= \frac{1}{2}\, exp(\frac{-x^2}{\epsilon}),\ x \in [0,1] \text{ and } \epsilon > 0\ ,
\end{aligned}$$

where we took $\epsilon = 0.01$.

4.1. **Estimation of parameters.** Whenever possible parameter values are estimated from available experimental data. However, given the large number of parameters in the model to be determined, it is perhaps not surprising that several remain unquantified. Focusing on the aim of our model which is to produce certain experimentally observed events of the urokinase plasminogen activation system in a *qualitative* manner, in the cases where no experimental data could be found, parameter values were chosen to give the best qualitative numerical simulation results. This is in line with previous papers successfully simulating tumour invasion and angiogenesis ([66], [16], [4], [23]).

4.1.1. *Estimation of the reference diffusion coefficients D, D_c, D_u.* We introduce D a reference chemical diffusion coefficient *e.g.* $D \sim 10^{-6} cm^2 s^{-1}$ ([14]). In their model of epidermal wound healing Sherratt and Murray ([75]), used values of $3\times10^{-9} cm^2 s^{-1}$ - $5.9\times10^{-11} cm^2 s^{-1}$ for the random motility of epidermal cells. Furthermore, in their study of individual endothelial cells (ECs), Stokes *et al.* ([77]) calculated a random motility coefficient of $(7.1 \pm 2.7)\times10^{-9} cm^2 s^{-1}$ for ECs migrating in a culture containing an angiogenic factor αFGF, heparin and fetal serum as well as a random motility coefficient of migrating endothelial cells with agarose overlays $(2.3 \pm 0.6)\times10^{-9} cm^2 s^{-1}$ and without agarose overlays of $(6.9 \pm 2.6)\times10^{-9} cm^2 s^{-1}$. In agreement with the aforementioned measurements for cell dispersion Bray ([14]) estimated the animal cell random motility coefficient to be $\sim 5 \times 10^{-10} cm^2 s^{-1}$. In this regard, our choice for cell dispersion will vary betweeen $10^{-9} cm^2 s^{-1}$ and $10^{-11} cm^2 s^{-1}$, so our nondimensional value will be between: $D_c = 10^{-3} - 10^{-5}$.

For the diffusion coefficient of the chemotactic chemical, Sherratt and Murray ([75]) took values of $3.1 \times 10^{-7} cm^2 s^{-1}$- $6.9 \times 10^{-6} cm^2 s^{-1}$ for an activator and inhibitor chemical respectively while Chaplain *et al.* ([21]) chose $3.3\times10^{-8} cm^2 s^{-1}$. Assuming that the diffusion coefficient of a diffusible chemical is in the range $10^{-6} - 10^{-9} cm^2 s^{-1}$, we obtain a dimensionless estimate of D_u in the range 0.001 - 1.

4.1.2. *The chemotactic (χ_c) and the haptotactic (ξc) coefficients.* Stokes *et al.* (1991) estimated the chemotaxis coefficient of ECs migrating in a culture containing αFGF, to be $2600 cm^2 s^{-1} M^{-1}$. Andreasen *et al.* ([6]) estimated the blood plasma concentration of uPA to be around $20pM$ while Collen *et al.* (1986) considered a uPA concentration around $8nM$ in his studies. Choosing χ_c between 0.001 - 1 gives a value of u_o in the range $0.38 \times 10^{-9} M - 0.38 \times 10^{-12} M$ which is consistent with experimental measurements. In the absence of reliable empirical data, we chose the haptotaxis coefficient ξ_c to be in the range of $2.5 \times 10^{-3} - 2.5 \times 10^{-1}\, cm^2 s^{-1} M^{-1}$. Therefore, considering the fact that the vitronectin blood plasma concentration is around $4\mu M$ (Comper, 1985) leads to a dimensionless estimate of the haptotaxis coefficient ξ_c in the range between 0.001 - 1.

4.1.3. *Proliferation rate constant, μ_1.* Yu *et al.* ([85]) estimated the doubling time of human epidermoid carminoma cells (HEp3) from *in vitro* proliferation experiments time to be $24h$. However, small differences in growth rate were observed but they did not bear a relation to the level of the uPAR. In contrast, HEp3 with a full uPAR complement grows best when crowded. By taking the proliferation rate as the reciprocal of the cell-cycle time we get $\tilde{\mu}_1 \sim 0.042 h^{-1}$.

Previously, Sherratt and Murray ([75]) as well as Stokes and Lauffenburger ([77]) estimated the growth rate constant to be $0.04h^{-1}$ and $0.056h^{-1}$ respectively, assuming that all cells are proliferating. Nevertheless, Stokes and Lauffenburger ([77]),

[21]), as well as Orme and Chaplain ([66]), reduced the chosen value of the proliferation rate to be $0.02h^{-1}$ in order for them to compensate with the assumption that fibronectin can inhibit endothelial cell proliferation and furthermore that during the angiogenesis process proliferation is mainly confined to a zone just proximal to the tips of the capillary sprouts.

In this regard, in our numerical simulations we will choose the proliferation rate to be between $0.02h^{-1} - 0.72h^{-1}$, and thus obtain the dimensionless parameter of μ_1 in the range 0.05 - 2.

4.1.4. *uPA neutralisation.* It is possible to estimate the parameter β from experimental data. We estimate β in the case of uPA by using experimental data on uPA-bound uPAR. Estreicher *et al.* ([37]) have shown that receptor-bound uPA remains exposed at the cell-surface with a half-life of 4-5 h, while Blasi *et al.* ([13]) calculated that bound uPA does not dissociate rapidly from the cell surface ($t_{1/2} > 5h$), nor is it appreciably endocytosed and/or degraded. These results extend the observations of Stoppeli *et al.* ([79]) and Bajpai and Baker ([11]) who had reported that a large fraction of uPA is accessible to trypsin or acid elution $2 - 4h$ after binding to the cells. However, the slow endocytosis of uPA is in contrast to the rapid internalization of other ligands of cell surface receptors present on the same cell, for example insulin. In this regard, considering $t_{1/2} = \frac{ln2}{\beta}$ ([8]), and since the uPA half-life time is estimated between $2 - 5h$ we thus choose the dimensionless estimate of $\beta \approx 0.13 - 0.95$.

4.1.5. *Remaining Parameters.* There were a couple of parameters in the model that we were unable to estimate. Therefore, we chose their values in order to give the best qualitative results in the simulations. Considering the uPA secretion from the cancer cells we chose the nondimensional value of α to vary between 0.05 - 1, whereas for the extracellular matrix degradation rate we consider δ to vary between 1 - 20. Furthermore, we chose the extracellular matrix remodelling rate to be three to five times higher than the cancer cells proliferation rate, and therefore we took μ_2 in the range of 0.15 - 2.5. Last but not least, we consider $\tau = 10^4 seconds$.

5. **Numerical results for the PDE model.** To compute numerical solutions of our model in one space dimension we use the NAG library subroutine D03PCF. This method uses finite difference approximations to perform a spatial discretisation of the model equations, thereby reducing them to a system of (time-dependent) ordinary differential equations which are readily integrated (this is the method of lines). The (stiff) ODE system is solved using a backward difference formula.

5.1. **Haptotaxis-only model.** In this section we will focus on the role of haptotaxis in the cancer invasion of tissue. As has already been described previously in the paper cancer cell membrane receptors (such as uPAR) can bind to ECM components (such as VN) and either degrade them through the activation of several proteases (such as uPA) or use them in order to move to distant sites. On the other hand, uPA production supports uPAR and VN binding. In this regard, we will try to clearly demonstrate these important interactions using as a basis the following theoretical framework, which focuses on haptotaxis as the dominant mechanism for

the movement of the cancer cells:

$$\begin{aligned}
\frac{\partial c}{\partial t} &= \underbrace{\nabla\cdot(D_c\nabla c)}_{\text{dispersion}} - \underbrace{\nabla\cdot(\xi_c c\nabla v)}_{haptotaxis} + \underbrace{\mu_1\, c\,(1-c-v)}_{proliferation}\,, \\
\frac{\partial v}{\partial t} &= \underbrace{-\delta\, u\, v}_{proteolysis} + \underbrace{\mu_2\, v\,(1-c-v)}_{renewal}\,, \qquad (9)\\
\frac{\partial u}{\partial t} &= \underbrace{D_u\,\nabla^2 u}_{diffusion} + \underbrace{\alpha\, c}_{production} - \underbrace{\beta\, u}_{decay}\,.
\end{aligned}$$

In order for us to to solve the system (9), we impose the boundary conditions presented by the equations (6) and (7) and we consider the initial conditions prescribed by the system (8). Additionally, to obtain the following simulations we used the following dimensionless parameter values: $D_c = 10^{-4}, D_u = 10^{-2}, \chi_c = 0, \xi_c = 5\times 10^{-3}, \alpha = 0.05, \beta = 0.3, \delta = 10, \mu_1 = \mu_2 = 0, L = 0.1cm, \tau = 10^4 sec$ (unless specified otherwise).

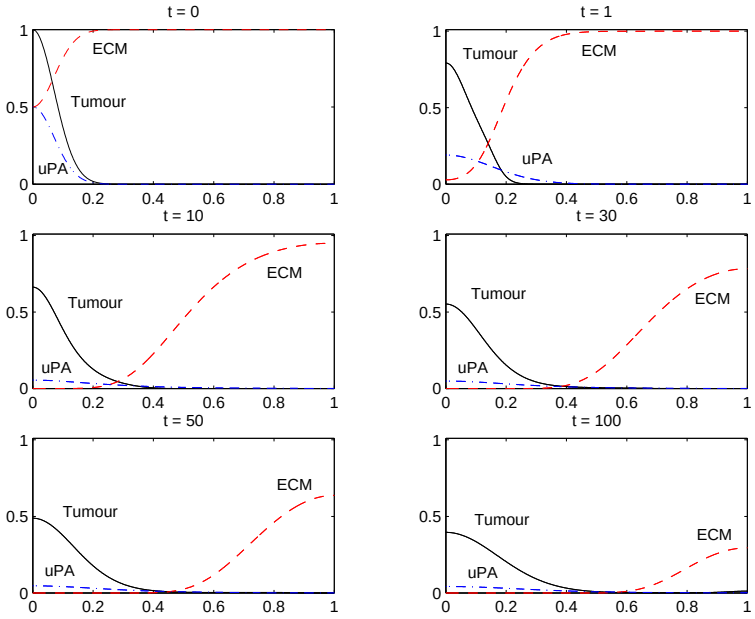

FIGURE 1. *Sequence of profiles showing the evolution of the tumour cell density $c(x,t)$ (solid black line), the protease concentration $u(x,t)$ (dot-dashed blue line) and the ECM density $v(x,t)$ (dashed red line), in which haptotaxis dominates the cancer cells' directed movement. Parameter values: $D_c = 10^{-4}, D_u = 10^{-2}, \xi_c = 0.05, \chi_c = 0, \alpha = 0.05, \beta = 0.3, \delta = 10, \mu_1 = \mu_2 = 0, L = 0.1cm, \tau = 10^4 sec$.*

In Figure 1, six snapshots in time of the tumour cell density, extracellular matrix (ECM) density and the uPA concentration are presented. Initially, by $t = 1$ (~ 3 hours) cancer cells have migrated a small distance into the domain. By $t = 30$ ($\sim$ 3.5 days), (low densities of) cancer cells have migrated almost half way through the

domain due to VN-mediated migration. Therefore, as time evolves by $t = 100$ ($\sim$ 11 days) cancer cells continue to migrate to regions where high ECM densities are situated.

In Figure 2 we increase the haptotactic coefficient ξ_c by a factor of 10, i.e. $\xi_c = 5 \times 10^{-2}$ (all other parameters remain unchanged from Figures 1). The tumour cell density distribution at $t = 1$ ($\sim$ 3 hours), in Figure 2, shows that a rather large cluster of cells has built up at the leading edge of the tumour due to increased haptotactic migration. By the time $t = 9$ ($\sim$ 1 day) this initial cluster of cells reach the right-hand boundary. In this regard we assume that the right-hand boundary represents a region of hard tissue or bone that the cancer cells are unable to penetrate (zero flux boundary conditions) and thus they start to move in the opposite direction to their initial direction, driven mainly by haptotaxis in response to the undegraded extracellular matrix components gradient. This becomes even more apparent in Figure 3.

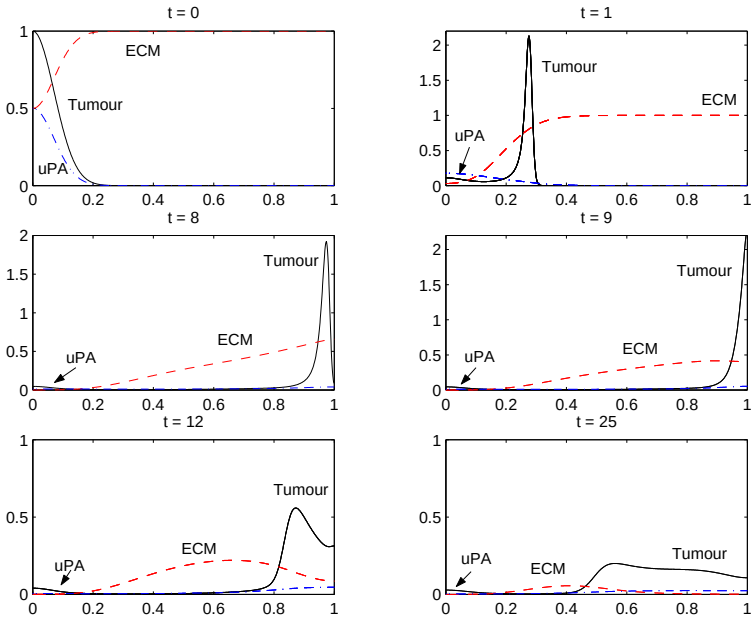

FIGURE 2. *Sequence of profiles showing the evolution of the tumour cell density $c(x,t)$ (solid black line), the protease concentration $u(x,t)$ (dot-dashed blue line) and the ECM density $v(x,t)$ (dashed red line), with increased haptotactic coefficient. Cancer cells invade the degraded ECM and a large cluster of cancer cells has formed at the tumour front which migrate further as time evolves. Parameter values:* $D_c = 10^{-4}, D_u = 10^{-2}, \xi_c = 0.05, \chi_c = 0, \alpha = 0.05, \beta = 0.3, \delta = 10, \mu_1 = \mu_2 = 0, L = 0.1cm, \tau = 10^4 sec.$

In Figure 3 we increase the haptotactic coefficient even further *i.e.* $\xi_c = 1 \times 10^{-1}$. At $t = 1$ ($\sim$ 3 hours), there is a large cluster of cells which has migrated from the main body of the tumour. Comparing the plot at $t = 6$ ($\sim$ 16 hours) in Figure 3 with that at $t = 9$ ($\sim$ 25 hours) in Figure 2, we see that cell migration is now much faster, as expected due to the increased haptotactic coefficient. However, by the

time that this invading cluster of cells reaches the right-hand boundary (which as in Figure 2 may be taken to represent a region of hard tissue or bone, that the cancer cells are unable to penetrate) they once again start ($t = 9$, ($\sim$ 25 hours)) to move backwards into the tissue space driven mainly by haptotaxis and the remaining (undegraded) extracellular components.

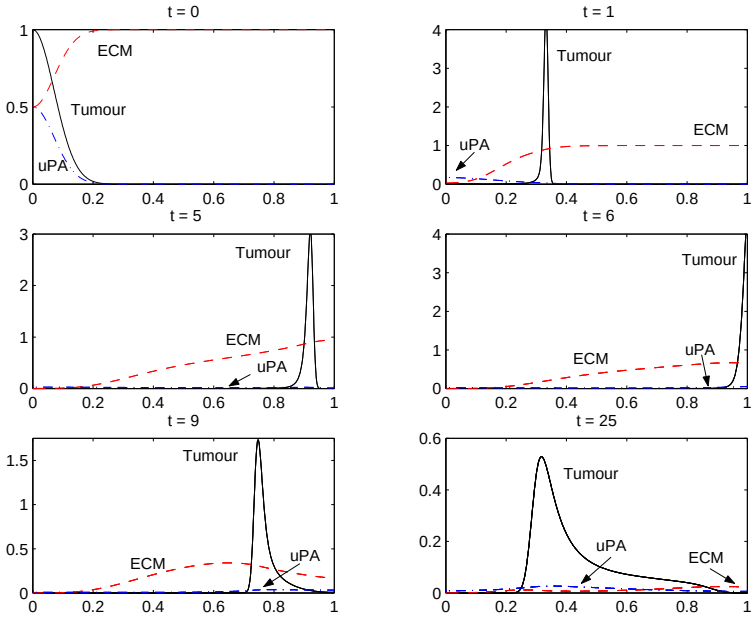

FIGURE 3. *Sequence of profiles showing the evolution of the tumour cell density $c(x,t)$ (solid black line), the protease concentration $u(x,t)$ (dot-dashed blue line) and the ECM density $v(x,t)$ (dashed red line), with increased haptotactic coefficient. Cancer cells invade the degraded ECM and a large cluster of cancer cells has formed at the tumour front which migrate further as time evolves. Parameter values:* $D_c = 10^{-4}, D_u = 10^{-2}, \chi_c = 0, \xi_c = 0.1, \alpha = 0.05, \beta = 0.3, \delta = 10, \mu_1 = \mu_2 = 0, L = 0.1cm, \tau = 10^4 sec.$

Having examined the previously described Figures 1 to 3 we note that invasion must be properly controlled. Therefore, in Figure 1 we had poor invasion due to the fact that the extracellular matrix was degraded too quickly. On the contrary, in Figures 2 and 3 cancer cells can respond more quickly to the gradients and therefore invasion is successful. Indeed the results of Figures 2 and 3 show that cancer cells may move backwards following the extracellular matrix components gradient.

We now consider a number of combined changes. We consider the effect of the proliferation of the cancer cells and the remodelling of the extracellular matrix components (*i.e.* $\mu_1 = 0.5$ $\mu_2 = 1.25$) in the model. Additionally, since directed cell migration requires localized proteolysis, and polarized expression of the uPA receptor could be a way to focus plasmin-mediated extracellular matrix degradation to the leading edge of migrating cancer cells therefore we included the term $\alpha c(1-c)$ in the uPA evolution equation (3) in order to "polarize" the uPA production at the

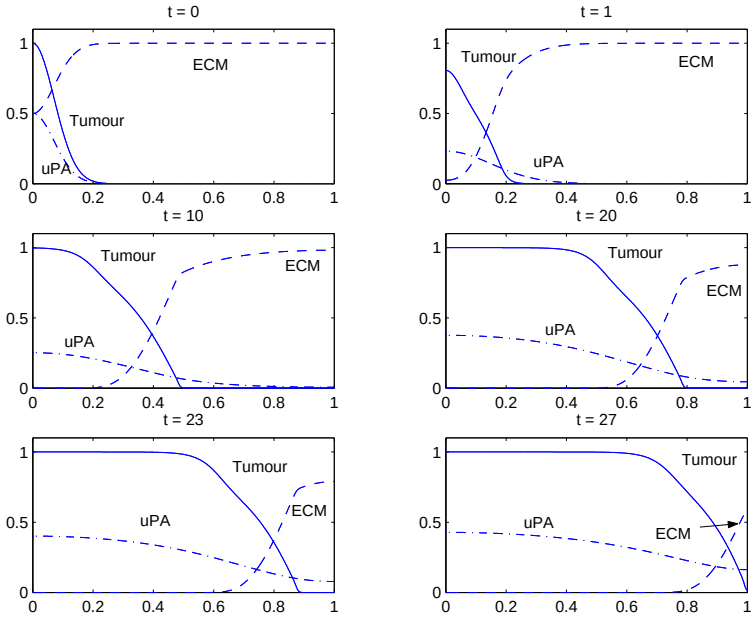

FIGURE 4. *Sequence of profiles showing the evolution of the tumour cell density $c(x,t)$ (solid black line), the protease concentration $u(x,t)$ (dot-dashed blue line) and the ECM density $v(x,t)$ (dashed red line), for which successful invasion occurs and a travelling wave which propagates into the tissue is established. Parameter values: $D_c = 10^{-4}, D_u = 10^{-2}, \chi_c = 0, \xi_c = 5 \times 10^{-3}, \alpha = 0.075, \beta = 0.15, \delta = 10, \mu_1 = 0.5, \mu_2 = 1.25, L = 0.1cm, \tau = 10^4$.*

invading leading edge (Estreicher *et al.*, 1990, [16]). Therefore, system (9) takes the following form:

$$\begin{aligned}
\frac{\partial c}{\partial t} &= \underbrace{\nabla \cdot (D_c \nabla c)}_{\text{dispersion}} - \underbrace{\nabla \cdot (\chi_c c \nabla v)}_{haptotaxis} + \underbrace{\mu_1\, c\, (1 - c - v)}_{proliferation}, \\
\frac{\partial v}{\partial t} &= \underbrace{-\delta\, u\, v}_{proteolysis} + \underbrace{\mu_2\, v\, (1 - c - v)}_{renewal}, \qquad (10) \\
\frac{\partial u}{\partial t} &= \underbrace{D_u\, \nabla^2 u}_{diffusion} + \underbrace{\alpha\, c\, (1 - c)}_{production} - \underbrace{\beta\, u}_{decay}\ .
\end{aligned}$$

We use the same initial and boundary conditions considered for system (9) while also regarding the Figure 4 we have increased the uPA production rate $\alpha = 0.075$ and we have decreased the uPA decay rate as well $\beta = 0.15$ (all other parameters having the same value as in Figure 1).

In Figure 4, we note that by $t = 1$ (~ 3 hours) a cluster of cells has built up at the tumour leading edge. By $t = 10$ (~ 1 day) this cluster of cells has migrated almost half way through the domain driven by the ECM-mediated haptotaxis. In other words, uPA is produced by the cancer cells at the leading edge and thus degrades the ECM at the invading leading front. The cancer cells haptotactically migrate into

the region of degraded tissue in response to the gradient in v. By $t = 27$ (~ 3 days) cancer cells have migrated almost all the way through the degraded extracellular milieu.

Next the results shown in Figure 5 consider the same combined changes with those discussed in Figure 4. However, in addition we also consider the effect of increased haptotaxis coefficient (*i.e.* $\xi_c = 0.0075$) as well as the effect of increased cancer cell proliferation and tissue remodelling rate (*i.e.* $\mu_1 = 0.75$, $\mu_2 = 3.5$, all other parameters having the same value as for Figure 4). Comparing the plot at $t = 10$ (~ 1 day) with that in Figure 4, we see that cancer cell invasion is now faster, as is to be expected, due to the increased haptotactic coefficient that we considered. Therefore, by $t = 30$ (~ 3.5 days), in Figure 5, cancer cells have migrated all the way through the domain.

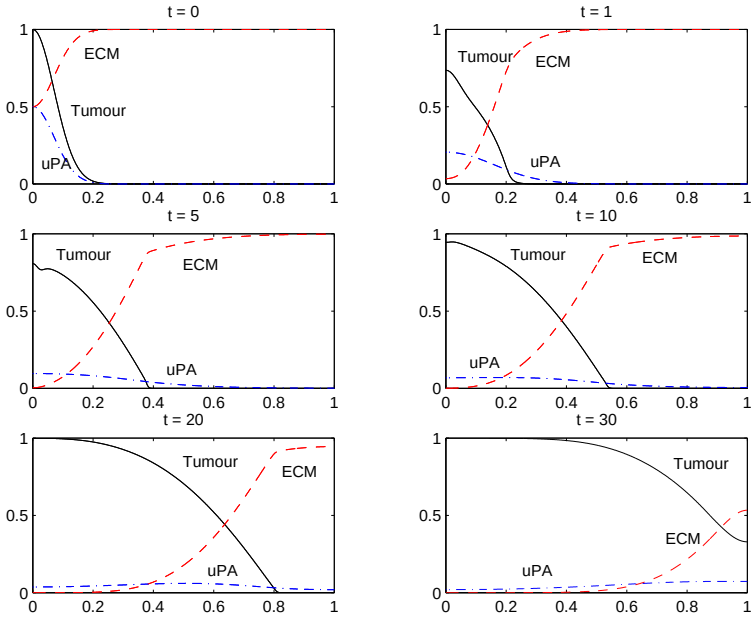

FIGURE 5. *Sequence of profiles showing the evolution of the tumour cell density $c(x,t)$ (solid line), the protease concentration $u(x,t)$ (dot-dashed line) and the ECM density $v(x,t)$ (dashed line), for which successful invasion occurs and a travelling wave which propagates into the tissue is established. Parameter values:* $D_c = 10^{-4}, D_u = 10^{-2}, \chi_c = 0, \xi_c = 0.0075, \alpha = 0.075, \beta = 0.15, \delta = 10, \mu_1 = 0.75, \mu_2 = 3.5, L = 0.1cm, \tau = 10^4 sec.$

In Figures 6 and 7 we consider the effect that combined changes to several terms could have on the model results. In this regard, several studies suggest that overexpression of uPA bound to the tumour cell-surface receptors leads to a signalling loop and/or activation of additional mechanisms related to this binding that contribute not only to enhanced pericellular proteolysis, survival and migration of the tumour cells, but surprisingly also to tumour growth and proliferation ([1]). Therefore, we introduce the term γuc in both the cancer cell equation and the uPA

equation representing cancer cell proliferation γuc and uPA neutralization $-\gamma uc$ respectively.

Recent evidence from Bafetti *et al.* (1998) indicate that vitronectin may induce the secretion of several proteases (MMP-2, uPA) in B16F1 and B16F10 cells while Khan and Falcone (1997) demonstrate that macrophage expression of uPA and MMP-9 is up-regulated when cultured on basement membrane extracts. In this regard, we consider the term αcv as a representation of uPA production through the cell-matrix signalling cascade. This term has also been considered by Perumpanani and Byrne (1999).

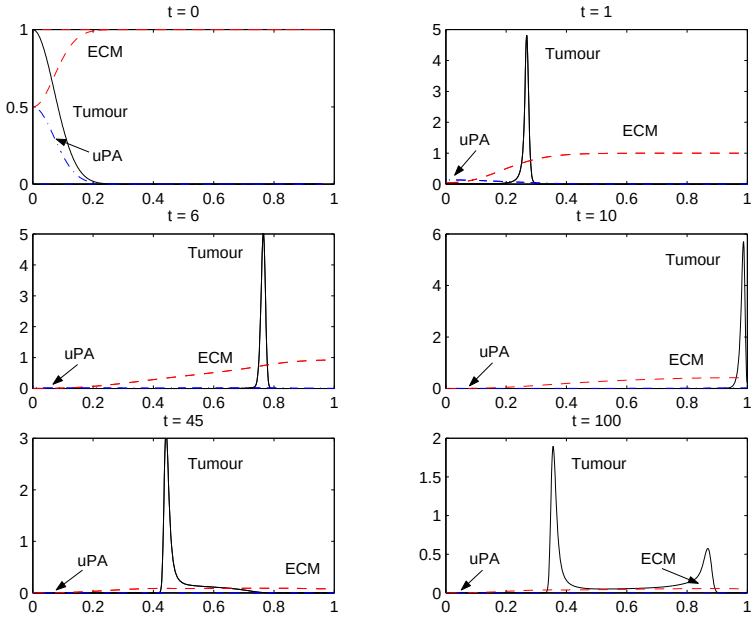

FIGURE 6. *Sequence of profiles showing the evolution of the tumour cell density $c(x,t)$ (solid black line), the protease concentration $u(x,t)$ (dot-dashed blue line) and the ECM density $v(x,t)$ (dashed red line), for which successful invasion and metastasis occur when we consider $D(c,u,v) = D_c(1+uv)$, $\xi = \xi_c \frac{\kappa_1}{(\kappa_2+\kappa_3 v)^2}$, and (γuv). Parameter values: $D_c = 10^{-5}, D_u = 15\times 10^{-3}, \xi_c = 15\times 10^{-2}, \alpha = 0.05, \beta = 0.3, \gamma = 0.15, \delta = 10, \mu_1 = \mu_2 = 0, \kappa_{1,2,3} = 1, L = 0.1cm, \tau = 10^4 sec.$*

Moreover, regarding the haptotactic function $\xi_c(v)$ we consider the function $\frac{\kappa_1}{(\kappa_2+\kappa_3 v)^2}$ representing the desensitization of cancer cells in response to a dense extracellular matrix ([54], [20], [76], [22]). Additionally, we consider a nonlinear diffusion term $D(c,u,v) = D_c\,(1+uv)$ representing the increased cell random movement towards regions where high amounts of uPA and VN are situated.

Considering all of the above combined changes, our modifies haptotaxis-only model now takes the following form:

$$\begin{aligned}
\frac{\partial c}{\partial t} &= \underbrace{\nabla\cdot(D_c\nabla c)}_{\text{dispersion}} - \underbrace{\nabla\cdot(\xi_c\frac{\kappa_1}{(\kappa_2+\kappa_3 v)^2}c\nabla v)}_{haptotaxis} + \underbrace{\gamma\, cu}_{proliferation} \quad , \\
\frac{\partial v}{\partial t} &= \underbrace{-\delta\, u\, v}_{proteolysis} \quad , \\
\frac{\partial u}{\partial t} &= \underbrace{D_u\nabla^2 u}_{diffusion} + \underbrace{\alpha\, c\, v}_{production} - \underbrace{\beta\, u}_{decay} - \underbrace{\gamma\, u\, c}_{binding} \quad ,
\end{aligned} \tag{11}$$

Subjest to the initial and boundary conditions presented by the equations (6)-(7) and system (8) respectively. Additionally, to obtain the following simulations we used the following dimensionless parameter values: $D_c = 10^{-4}, D_u = 15\times 10^{-3}, \chi_c = 0, \xi_c = 15\times 10^{-2}, \alpha = 0.05, \beta = 0.3, \gamma = 0.15, \delta = 10, \mu_1 = \mu_2 = 0, \kappa_1 = \kappa_2 = \kappa_3 = 1, L = 0.1cm, \tau = 10^4 sec$ (unless specified otherwise).

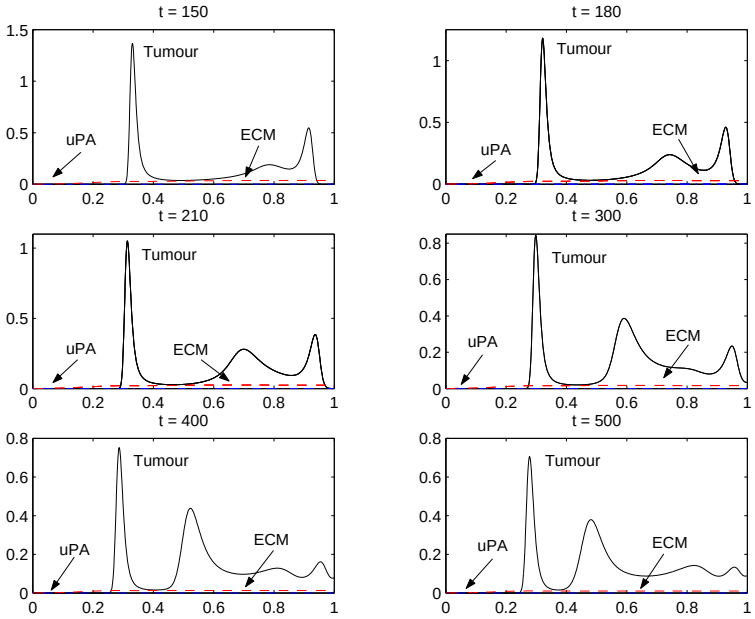

FIGURE 7. Sequence of profiles showing the evolution of the tumour cell density $c(x,t)$ (solid line), the protease concentration $u(x,t)$ (dot-dashed line) and the ECM density $v(x,t)$ (dashed line), for which successful invasion and metastasis occur when we consider $D(c,u,v) = D_c(1+uv)$, $\xi = \xi_c\frac{\kappa_1}{(\kappa_2+\kappa_3 v)^2}$, and neutralization/proliferation γuv. Parameter values: $D_c = 10^{-5}, D_u = 15\times 10^{-3}, \xi_c = 15\times 10^{-2}, \alpha = 0.05, \beta = 0.3, \gamma = 0.15, \delta = 10, \mu_{1,2} = 0, \kappa_{1,2,3} = 1, L = 0.1cm, \tau = 10^4 sec.$

The results are presented in the following Figures 6 and 7. By $t = 1$ ($\sim$ 3 hours) in Figure 6 a large cluster of cells has built up at the leading edge of the tumour

driven by both haptotaxis and haptokinesis. As time evolves, $t = 10$ ($\sim$ 1 day), this large cluster of cancer cells has already reached the right hand boundary which once again we assume represents hard tissue or bone that the cancer cells are unable to penetrate. Consequently, the cancer cells start to move backwards driven by the ECM-mediated haptotaxis and haptokinesis. In addition, at $t = 85$ ($\sim$ 10 days), two clusters of cells start to form, giving us the indication that the initial cluster of cells the may be able to break into two or more separate clusters, and therefore invade and metastasize to distant sites of the body.

As time evolves, at $t = 150$ ($\sim$ 17 days) in Figure 7, we note that a new cluster of cells start to form as a result of cancer cell proliferation. This is even more evident at $t = 300$ ($\sim$ 35 days) where three cluster of cells have formed. In additon, by $t = 500$ ($\sim$ 58 days) the cluster of cells situated near the right-hand boundary starts to migrate as a result of ECM mediated haptotaxis.

The results presented in the next set of Figures 8 and 9, arise from simulations of the modified system (11) with the only change being that we consider linear diffusion. Therefore, we solved the system (11) subject to the following parameter values: $D_c = 10^{-5}, D_u = 25 \times 10^{-3}, \xi = 0.1, \alpha = 0.05, \beta = 0.3, \delta = 10, \gamma = 0.075, \mu_1 = \mu_2 = 0, \kappa_{1,2,3} = 1, L = 0.1cm, \tau = 10^4 sec.$

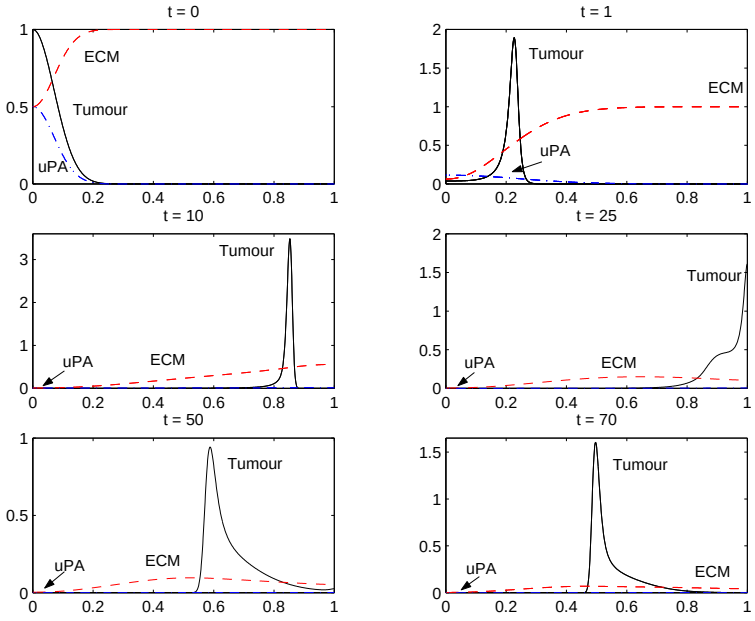

FIGURE 8. *Sequence of profiles showing the evolution of the tumour cell density $c(x,t)$ (solid black line), the protease concentration $u(x,t)$ (dot-dashed blue line) and the ECM density $v(x,t)$ (dashed red line), for which successful invasion and several metastases occur due to a receptor-kinetic haptotaxis function $\xi = \xi_c \frac{\kappa_1}{(\kappa_2+\kappa_3 v)^2}$, and neutralization/proliferation term γcu. Parameter values: $D_c = 10^{-5}, D_u = 25 \times 10^{-3}, \chi_c = 0, \xi_c = 1 \times 10^{-1}, \alpha = 0.05, \beta = 0.3, \delta = 10, \mu_1 = \mu_2 = 0, \gamma = 0.075, \kappa_{1,2,3} = 1, L = 0.1cm, \tau = 10^4 sec.$*

In Figure 8 we note that by $t = 1$ ($\sim$ 3 hours) a large group of cells has built up at the leading edge of the tumour. At $t = 10$ ($\sim$ 1 day) this large group of cells has migrated further into the region driven by the ECM-mediated haptotaxis. As time evolves, at $t = 30$ ($\sim$ 3.5 days), cancer cells have reached the right hand boundary and start to move backwards driven mainly by the ECM-mediated haptotaxis.

By $t = 100$ ($\sim$ 11.5 days) in Figure 9 this large cluster of cells is situated in the centre of the domain and at $t = 130$ ($\sim$ 15 days) a new group of cancer cells start to form the secondary tumour. This new cluster of cancer cells is building up the leading front of the secondary tumour and starts to migrate towards the right hand boundary driven by the ECM mediated haptotaxis. As time evolves, at $t = 380$ ($\sim$ 44 days) the two groups of cells start to migrate in different directions and therefore invade the rest of the remaining undegraded extracellular matrix components.

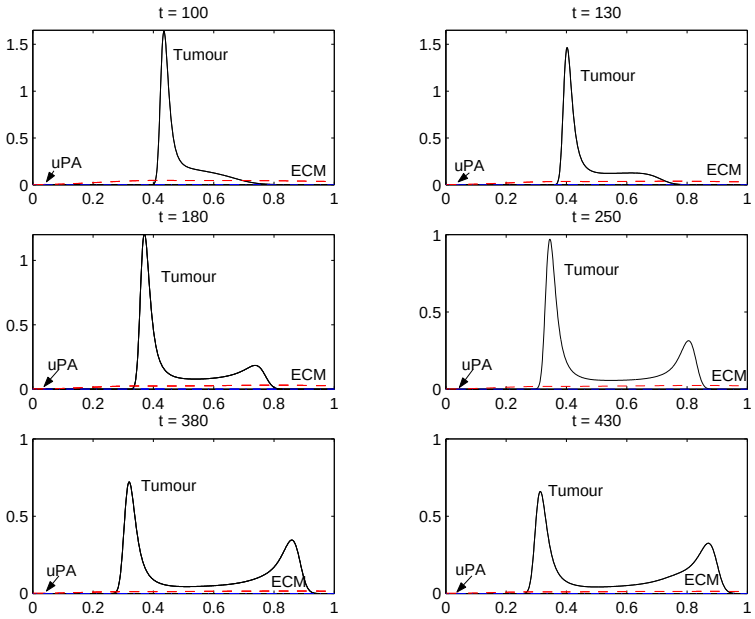

FIGURE 9. *Sequence of profiles showing the evolution of the tumour cell density $c(x,t)$ (solid black line), the protease concentration $u(x,t)$ (dot-dashed blue line) and the ECM density $v(x,t)$ (dashed red line), for which successful invasion and several metastases occur due to a receptor-kinetic haptotaxis function $\xi = \xi_c \frac{\kappa_1}{(\kappa_2+\kappa_3 v)^2}$, and neutralization/proliferation term γcu. Parameter values: $D_c = 10^{-5}, D_u = 25 \times 10^{-3}, \chi_c = 0, \xi_c = 1 \times 10^{-1}, \alpha = 0.05, \beta = 0.3, \delta = 10, \mu_1 = \mu_2 = 0, \gamma = 0.075, \kappa_{1,2,3} = 1, L = 0.1cm, \tau = 10^4 sec.$*

5.2. **A combined chemotactic - haptotactic model.** Since in the previous sections we focused our attention on the role of chemotaxis and haptotaxis individually, we now try to elucidate the motility-retarding or accelerating effects of uPA-chemotaxis and ECM-haptotaxis on the cancer cells invasion process. The demonstration that chemotaxis and haptotaxis operate through different receptors and have different signal transduction pathways has presented the possibility of two

separate targets to retard invasion. In this regard, we will now investigate the results when these two characteristic migrating mechanisms operate synchronously. Thus, the combined chemotaxis and haptotaxis theoretical framework is the following:

$$\begin{aligned}
\frac{\partial c}{\partial t} &= \underbrace{\nabla\cdot(D_c\nabla c)}_{\text{dispersion}} - \underbrace{\nabla\cdot(\chi_c c\nabla u)}_{chemotaxis} - \underbrace{\nabla\cdot(\xi_c c\nabla v)}_{haptotaxis} + \underbrace{\mu_1\, c\,(1-c-v)}_{proliferation}\,, \\
\frac{\partial v}{\partial t} &= \underbrace{-\delta\, u\, v}_{proteolysis} + \underbrace{\mu_2\, v\,(1-\,c-\,v)}_{renewal}\,, \qquad (12)\\
\frac{\partial u}{\partial t} &= \underbrace{D_u\,\nabla^2 u}_{diffusion} + \underbrace{\alpha\, c}_{production} - \underbrace{\beta\, u}_{decay}\,.
\end{aligned}$$

In order for us to to close the system (12), we impose the boundary conditions presented by the equations (6) and (7) and we consider the initial conditions prescribed by the system (8). Additionally, the following numerical results used the dimensionless parameter values below: $D_c = 10^{-4}, D_u = 10^2, \chi_c = 5\times10^{-3}, \xi_c = 5\times10^{-3}, \alpha = 0.05, \beta = 0.3, \mu_1 = \mu_2 = 0$.

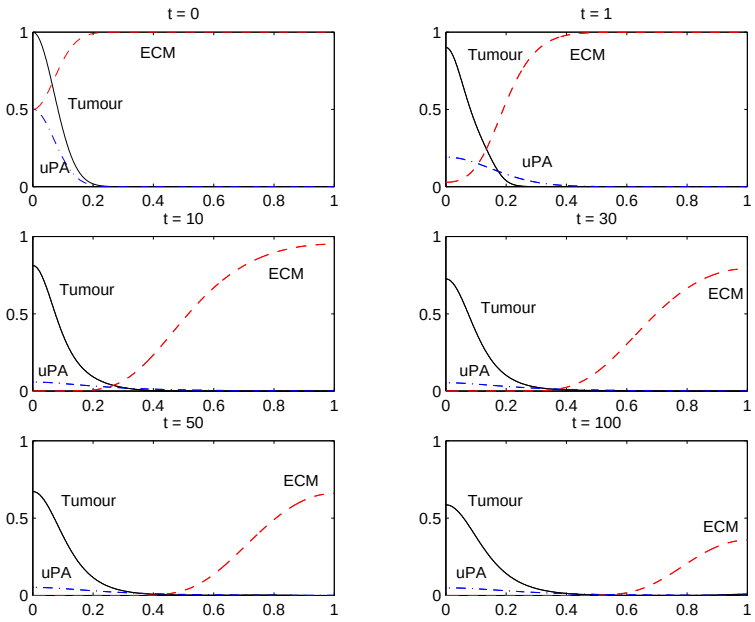

FIGURE 10. *Sequence of profiles showing the evolution of the tumour cell density $c(x,t)$ (solid line), the protease concentration $u(x,t)$ (dot-dashed line) and the ECM density $v(x,t)$ (dashed line). Parameter values: $D_c = 10^{-4}$, $D_u = 10^{-2}, \chi_c = \xi_c = 5\times10^{-3}, \alpha = 0.05$, $\beta = 0.3, \delta = 10, \mu_1 = 0 = \mu_2, L = 0.1cm, \tau = 10^4 sec$.*

With all the parameter values as above, we produce the plots given in Figure 10. In Figure 10 chemotaxis and the uPA-gradient direct cancer cells towards regions of high uPA concentration, whereas on the other hand haptotaxis and ECM-gradient directs cancer movement to regions of high extracellular matrix density. Therefore,

by $t = 1$ ($\sim$ 3 hours) cancer cells have migrated only a short distance in the domain, while by $t = 50$ ($\sim$ 6 days) cancer cells have migrated almost half the way into the domain, as a result, of course, of the oppositely directed uPA and ECM gradients.

In Figures 11 and 12 we examine the effect of increasing both the chemotactic coefficient (χ_c) and the haptotactic coefficient (ξ_c) by a factor of 10, *i.e.*, $\xi_c = 5 \times 10^{-2}, \chi_c = 5 \times 10^{-2}$ (all other parameters remain unchanged from Figure 10).

By $t = 1$ (3 hours), in Figure 11 we note that a large cluster of cells has built-up at the leading edge of the tumour. Comparing the plot at $t = 8$ ($\sim$ 3 hours), in Figure 11 with that in Figure 2, we see that the cancer cells driven both by haptotaxis and chemotaxis migrate at a slightly slower rate than those driven by haptotaxis alone. This is a consequence of the uPA chemotaxis, namely the uPA gradient slows the migration of the cancer cells towards the ECM due to their opposite directions. Therefore, at $t = 9$ ($\sim$ 1 day), in Figure 11, we note that two separate cluster of cells are formed near each boundary. This is because the initial cluster of cells remains near the left hand boundary as a result of increased levels of uPA in this region while the second cluster of cells is situated near the right hand boundary driven mainly by the ECM-mediated haptotaxis.

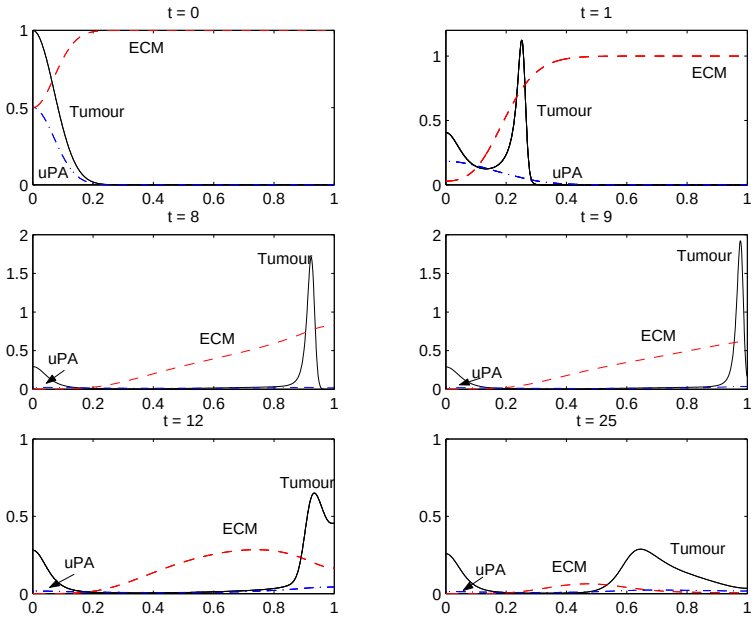

FIGURE 11. *Sequence of profiles showing the evolution of the tumour cell density $c(x,t)$ (solid black line), the protease concentration $u(x,t)$ (dot-dashed blue line) and the ECM density $v(x,t)$ (dashed red line), showing the effect of increasing χ as well as ξ by a factor of 10. Parameter values: $D_c = 10^{-4}, D_u = 10^{-2}, \chi_c = \xi_c = 5 \times 10^{-2}, \alpha = 0.05, \beta = 0.3, \delta = 10, \mu_1 = 0 = \mu_2, L = 0.1cm, \tau = 10^4 sec.$*

In addition, by the time that this initial cluster of cells reaches the right-hand boundary (at $t = 12$ ($\sim$ 1.5 days) in Figure 11, which as has already been mentioned earlier, could represent a region of hard tissue or bone) cancer cells start to move

backwards (with regards to their initial direction) driven by the ECM-mediated haptotaxis. As time evolves, at $t = 85$ ($\sim$ 10 days) two separate cluster of cells have formed, one near the left-hand boundary and the other almost in the centre of the domain. By $t = 155$ ($\sim$ 18 days), both cluster of cells remain in the position that they used to occupy at $t = 85$ ($\sim$ 10 days). This is because of the absence of both uPA-mediated chemotaxis and ECM-mediated haptotaxis. However, as time evolves $t = 650$ ($\sim$ 75 days), the secondary metastatic cluster of cells starts its invasive process again driven by chemotaxis and the uPA gradient.

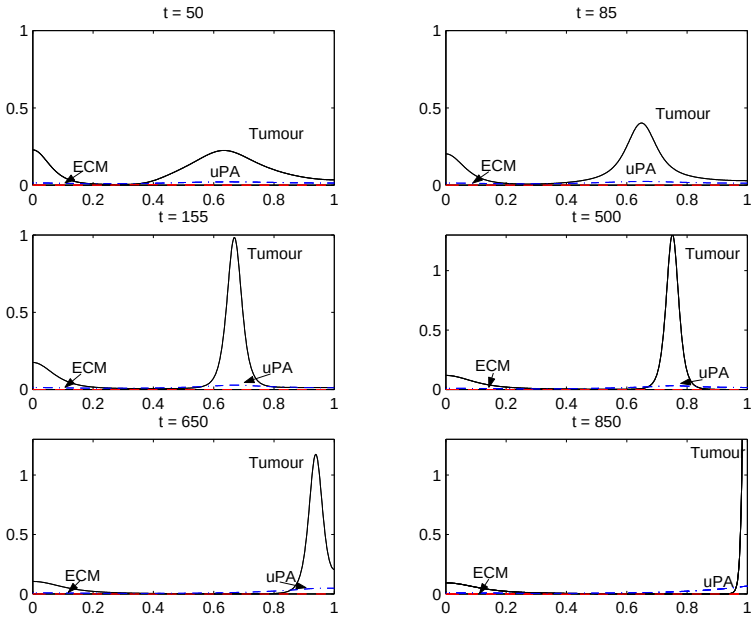

FIGURE 12. *Sequence of profiles showing the evolution of the tumour cell density $c(x,t)$ (solid black line), the protease concentration $u(x,t)$ (dot-dashed blue line) and the ECM density $v(x,t)$ (dashed red line), showing the effect of increasing χ as well as ξ by a factor of 10. Parameter values: $D_c = 10^{-4}, D_u = 10^{-2}, \chi_c = \xi_c = 5 \times 10^{-2}, \alpha = 0.05, \beta = 0.3, \delta = 10, \mu_1 = 0 = \mu_2, L = 0.1cm, \tau = 10^4 sec$.*

The influence of the proliferation function for both ECM and cancer cells is examined in the results in Figures 13 and 14, together with increased chemotactic and haptotactic coefficients (*i.e.* $\mu_1 = 0.15, \mu_2 = 0.75, \chi_c = 0.05, \xi_c = 0.065$, with all other parameters values as for Figure 10). In Figure 13, at $t = 1$ ($\sim$ 3 hours) we note that a large cluster of tumour cells has formed at the leading edge of the primary tumour. By $t = 5$, ($\sim$ 14 hours) cancer cells have migrated even further into the region driven mainly by haptotaxis. As time evolves, at $t = 30$ ($\sim$ 3.5 days) cancer cells have migrated into the whole domain while the rest of the extracellular matrix has been degraded.

At $t = 45$ ($\sim$ 5 days), in Figure 14, a new cluster of cancer cells is starting to form as a result of the cancer cell proliferation. By $t = 70$ ($\sim$ 8 days) the cancer cells start to migrate towards the right hand boundary driven by the uPA-chemotaxis

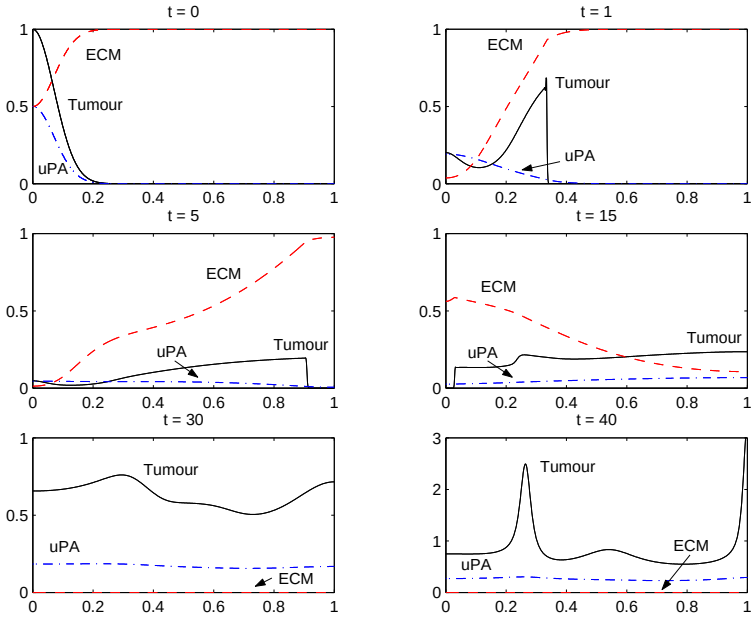

FIGURE 13. *Sequence of profiles showing the evolution of the tumour cell density $c(x,t)$ (solid black line), the protease concentration $u(x,t)$ (dot-dashed blue line) and the ECM density $v(x,t)$ (dashed red line), showing the effect of increasing χ_c, ξ_c as well as by increased proliferation in cancer invasion. Parameter values:* $D_c = 10^{-4}, D_u = 10^{-2}, \chi_c = 0.05, \xi_c = 0.065, \alpha = 0.1, \beta = 0.3, \delta = 10, \mu_1 = 0.15, \mu_2 = 0.75, L = 0.1cm, \tau = 10^4 sec.$

gradient. As time evolves, at $t = 100$ ($\sim$ 11.5 days), the previously mentioned cluster of cells has reached the right hand boundary while a new cluster of cells starts to form near the left hand boundary as a result of increased cell proliferation. The "*anarchy*" of the cancer cell cluster formation lies in the uPA-cancer cell surface receptors interactions and the increased level of cancer cell proliferation.

We now examine the effects that changing several key parameter values has on the solution. In particular, we consider the effect of increasing the cancer cell diffusion coefficient as well as decreasing the uPA diffusion coefficient, and the cancer cell and extracellular matrix proliferation and redistributuion rates respectively (*i.e.* $D_c = D_u = 0.001, \xi_c = 0.05, \chi_c = 0.3, \mu_1 = 0.05, \mu_2 = 0.1$). We note that, by $t = 1$ ($\sim$ 3 hours) a large cluster of cancer cells has built up at the leading edge of the primary tumour. As time evolves, $t = 10$ ($\sim$ 1 day) the invading cluster of cancer cells has migrated all the way through the domain driven mainly by VN-mediated haptotaxis. By $t = 35$ ($\sim$ 4 days), most of the extracellular matrix has been degraded and cancer cell locomotion is driven mainly by the uPA-mediated chemotaxis.

As time evolves, at $t = 45$ ($\sim$ 5 days), in Figure 16 we note that a rather large cluster of cells has formed at the center of the plot as a result of the cancer cell proliferation. By $t = 65$ ($\sim$ 7.5 days) we observe that a new cluster of cells start

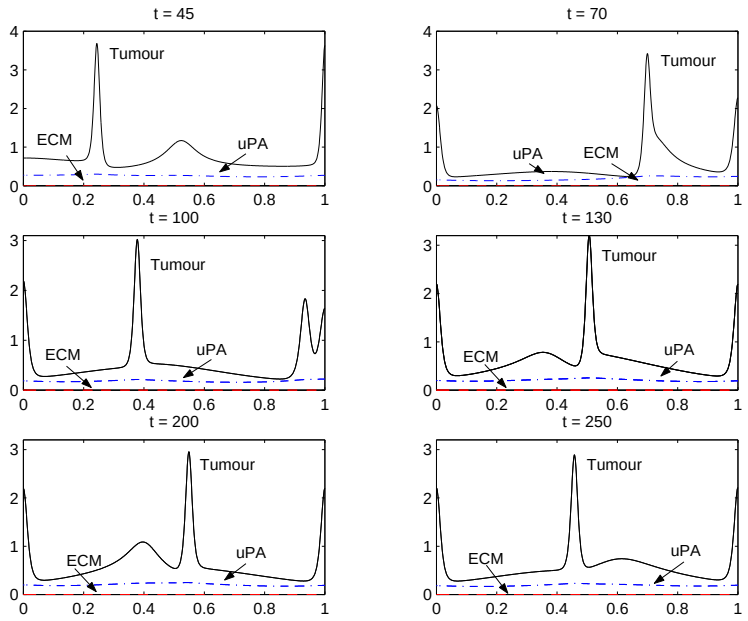

FIGURE 14. *Sequence of profiles showing the evolution of the tumour cell density $c(x,t)$ (solid black line), the protease concentration $u(x,t)$ (dot-dashed blue line) and the ECM density $v(x,t)$ (dashed red line), showing the effect of increasing χ_c, ξ_c as well as by increased proliferation in cancer invasion. Parameter values:* $D_c = 10^{-4}, D_u = 10^{-2}, \chi_c = 0.05, \xi_c = 0.065, \alpha = 0.1, \beta = 0.3, \delta = 10, \mu_1 = 0.15, \mu_2 = 0.75, L = 0.1cm, \tau = 10^4 sec.$

to form near the right hand boundary, and therefore by $t = 125$ ($\sim$ 14.5 days) two large cluster of cells have formed accompanied by increased levels of uPA.

In Figure 17, at $t = 130$ ($\sim$ 15 days) two large cluster of cells are formed. As time evolves, these three group of cells are static and a spatially heterogeneous profile/pattern is observed. Reminiscent perhaps of Turing-like instability. We will return to this in a latter chapter. Therefore, we could assume that in this stage the tumour is a dormant state. It has been observed ([1]) that the down-regulation of cell surface receptors, especially in human carcinoma cells, brings about a state of tumour dormancy. Especially in the absence of extracellular matrix components, the cell-ECM signalling cascade that regulates cancer cell *in vivo* growth switches to the "off" state and the cells become unable to grow *in vivo*.

5.3. **Incorporation of the plasminogen activation cycle.** In this section we will use a novel approach related either to the haptotactic function and/or the proliferation and degradation rates for cancer cells and the extracellular matrix respectively. As we have already seen in the previous sections, the uPA "life-cycle" has several stages such as:

- the production of the uPA by the cancer cells,
- the binding of uPA to uPAR,

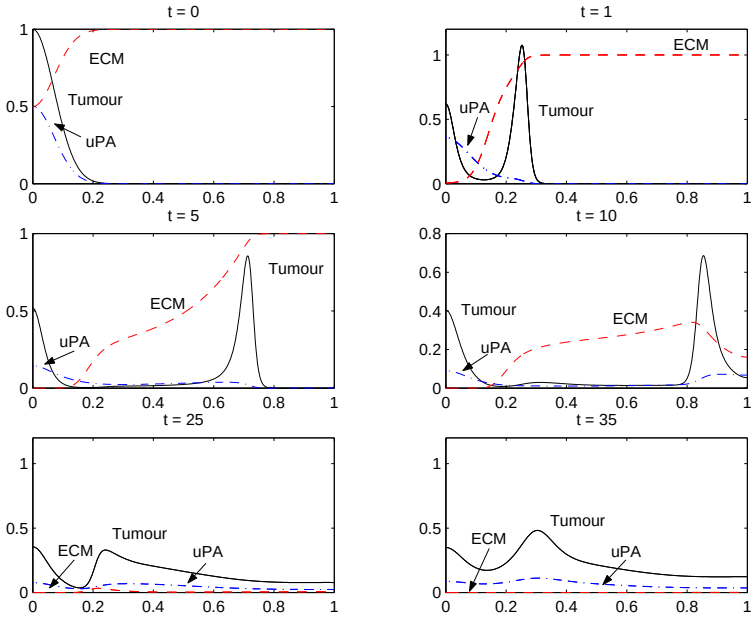

FIGURE 15. *Sequence of profiles showing the evolution of the tumour cell density $c(x,t)$ (solid black line), the protease concentration $u(x,t)$ (dot-dashed blue line) and the ECM density $v(x,t)$ (dashed red line), showing the effect of increasing D_c, and decreasing D_u and μ_1, μ_2 have in cancer invasion. Parameter values:* $D_c = 10^{-3}, D_u = 10^{-3}, \chi_c = 0.03, \xi_c = 0.05, \alpha = 0.1, \beta = 0.3, \delta = 10, \mu_1 = 0.05, \mu_2 = 0.1, L = 0.1cm, \tau = 10^4 sec.$

- and most important, the dormant stage of subsequent down regulation of uPAR and uPA respectively.

It is known that the uPA cycle is likely to possess (stable) limit cycle kinetics. In order to model this effect in the PDE system, we assume that the proliferation function is a function of a variable (e.g. uPAR) which has limit cycle kinetics. In order to capture this effect qualitatively, we choose the following system for the uPAR kinetics:

$$\begin{aligned} \frac{dp}{dt} &= q - 3 \\ \frac{dq}{dt} &= (q-3)(1-(p-2.1)^2) - (p-2.1) \end{aligned} \tag{13}$$

where p = uPA bound to the uPA receptor, and q = uPAR. This system 13 has limit cycle kinetics as shown in Figure 18. We now assume that, the cancer cell proliferation function as well as the extracellular matrix re-establishment function are given by:

$$\mu_c = \mu(u,c,v,p),\ \mu_v = \mu(u,c,v,p)$$

and therefore the corresponding proliferation terms are also "oscillating".

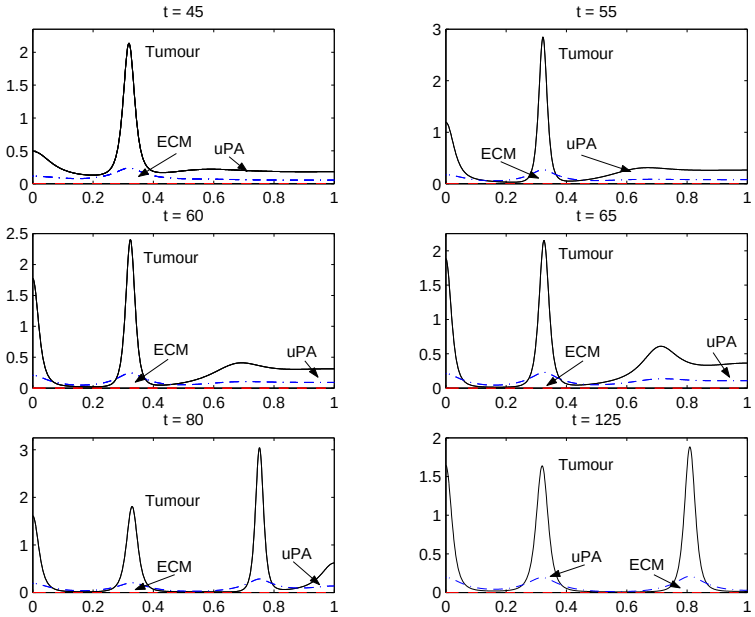

FIGURE 16. *Sequence of profiles showing the evolution of the tumour cell density $c(x,t)$ (solid black line), the protease concentration $u(x,t)$ (dot-dashed blue line) and the ECM density $v(x,t)$ (dashed red line), showing the effect of increasing D_c, and decreasing D_u and μ_1, μ_2 have in cancer invasion. Parameter values:* $D_c = 10^{-3}, D_u = 10^{-3}, \chi_c = 0.03, \xi_c = 0.05, \alpha = 0.1, \beta = 0.3, \delta = 10, \mu_1 = 0.05, \mu_2 = 0.1, L = 0.1cm, \tau = 10^4$.

In this regard, the combined full system of equations takes the following form:

$$
\begin{aligned}
\frac{\partial c}{\partial t} &= \underbrace{\nabla\cdot(D_c\nabla c)}_{\text{dispersion}} - \underbrace{\nabla\cdot(\chi_c c\nabla u)}_{chemotaxis} - \underbrace{\nabla\cdot(\xi_c c\nabla v)}_{haptotaxis} + \underbrace{\mu_1\, c p\,(1-c-v)}_{proliferation}\,, \\
\frac{\partial v}{\partial t} &= \underbrace{-\delta\, u\, v}_{proteolysis} + \underbrace{\mu_2\, v\, p\,(1-\,c-\,v)}_{renewal}\,, \qquad (14)\\
\frac{\partial u}{\partial t} &= \underbrace{D_u\nabla^2 u}_{diffusion} + \underbrace{\alpha\, c}_{production} - \underbrace{\beta\, u}_{decay}\,, \\
\frac{dp}{dt} &= q-3\,, \\
\frac{dq}{dt} &= (q-3)(1-(p-2.1)^2)-(p-2.1)\,.
\end{aligned}
$$

Therefore, by incorporating the aforementioned oscillatory behaviour in the cancer cells and extracellular matrix proliferation term we overcome a certain weakness of continuum models due to the fact that they normally only consider constant reproduction terms for cancer cells. In this regard, with the previously described inclusion we deduce that when cancer cells secrete uPA this will result in an increase in their proliferation rate while when there is a decay of uPA, *e.g.* due to

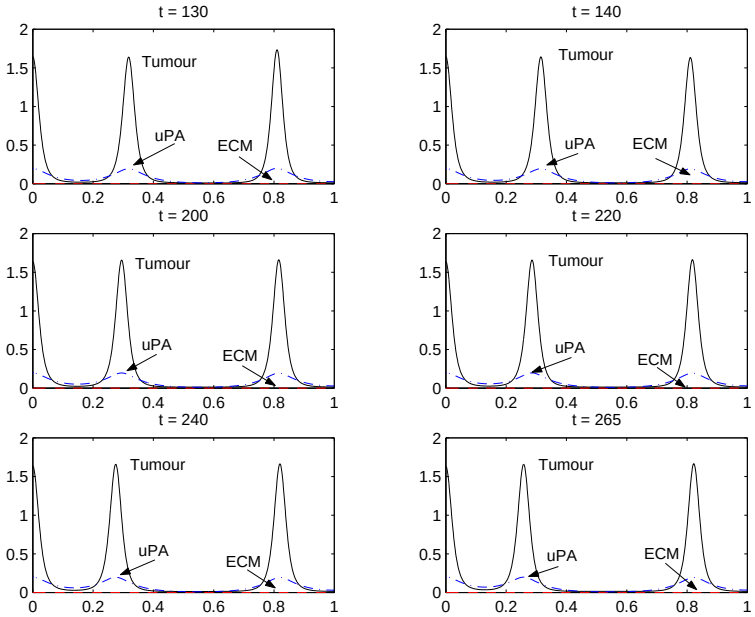

FIGURE 17. *Sequence of profiles showing the evolution of the tumour cell density $c(x,t)$ (solid black line), the protease concentration $u(x,t)$ (dot-dashed blue line) and the ECM density $v(x,t)$ (dashed red line), showing the effect of increasing D_c, and decreasing D_u and μ_1, μ_2 have in cancer invasion. Parameter values:* $D_c = 10^{-3}, D_u = 10^{-3}, \chi_c = 0.03, \xi_c = 0.05, \alpha = 0.1, \beta = 0.3, \delta = 10, \mu_1 = 0.05, \mu_2 = 0.1, L = 0.1cm, \tau = 10^4 sec.$

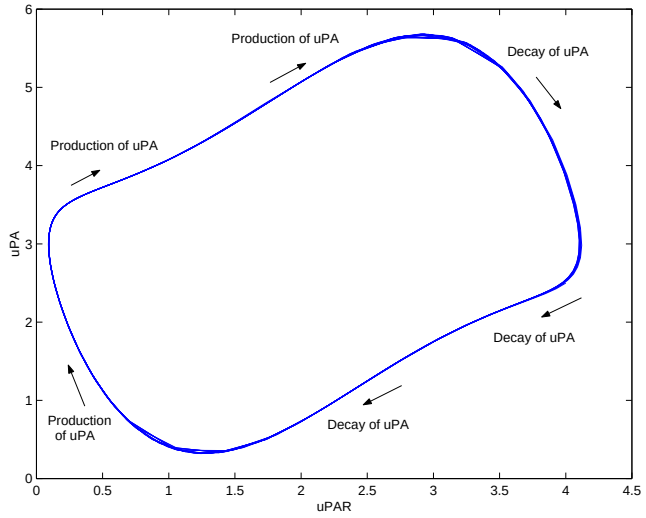

FIGURE 18. *Limit cycle kinetics for the urokinase plasminogen activation system.*

the presence of the inhibitors, the cancer cell proliferation rate will slow down. Figures 19 to 20 illustrate the results of the combined system (14).

We note that by $t = 1$ ($\sim$ 3 hours) in Figure 19 a large group of cancer cells has built up at the leading edge while by $t = 10$ ($\sim$ 1 day) this large group of cell has migrated all the way through the region. Comparing the plot at $t = 35$ ($\sim$ 4 days) in Figure 19, with that in Figure 15, we note the formation of a new cluster of cells, while in Figure 15 the formation of this new cluster of cells is observed later.

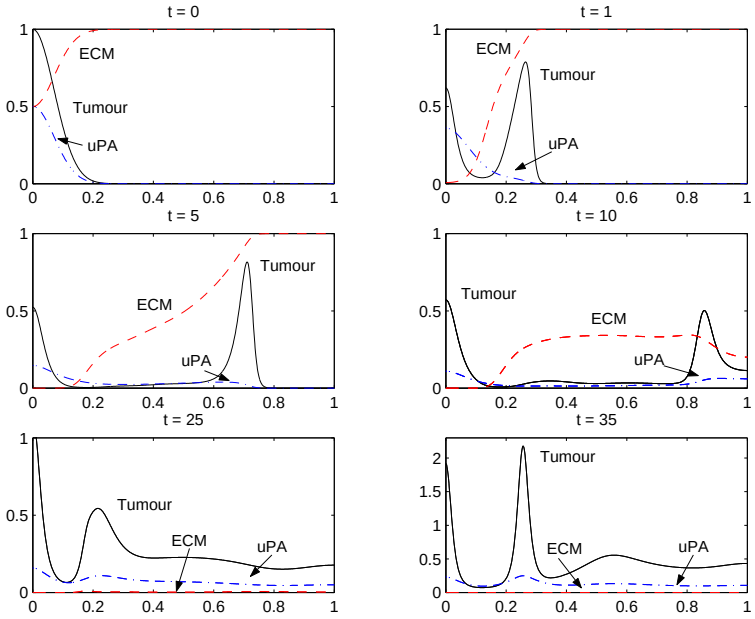

FIGURE 19. *Sequence of profiles showing the evolution of the tumour cell density $c(x,t)$ (solid black line), the protease concentration $u(x,t)$ (dot-dashed blue line) and the ECM density $v(x,t)$ (dashed red line), showing the effect of cycling proliferatinf rates. Parameter values:* $D_c = 10^{-3}, D_u = 10^{-3}, \chi_c = 0.03, \xi_c = 0.05, \alpha = 0.1, \beta = 0.3, \delta = 10, \mu_1 = 0.05, \mu_2 = 0.1, L = 0.1cm, \tau = 10^4 sec.$

As time evolves, at $t = 45$ ($\sim$ 5 days) two groups of cells are observed while at the same time in Figure 16 only a single large cluster of cells has formed. Considering the successive times between $t = 55$ (6$\sim$ days) to $t = 125$ ($\sim$ 14.5 days) we observe that the system remains in a "pause" state where the two cluster of cells are almost static. Therefore, we could once again assume that for several days the tumour in the absence of extracellular matrix which is vital for its movement components remains in an "*occult*" stationary state for several days ($\sim$ 8 days).

However, by $t = 130$ ($\sim$ 15 days), in Figure 21, the cluster of cells situated near the left hand boundary starts to migrate towards the left-hand boundary as a result of the uPA-mediated gradient. Therefore, by $t = 220$ ($\sim$ 25.5 days) the previously mentioned group of cells has migrated to the left-hand boundary, while a new group of cells has formed. By $t = 240$ ($\sim$ 28 days) the formation of two cluster of cells is evident while by $t = 225$ ($\sim$ 30 days) these two cluster of cells start to join to form

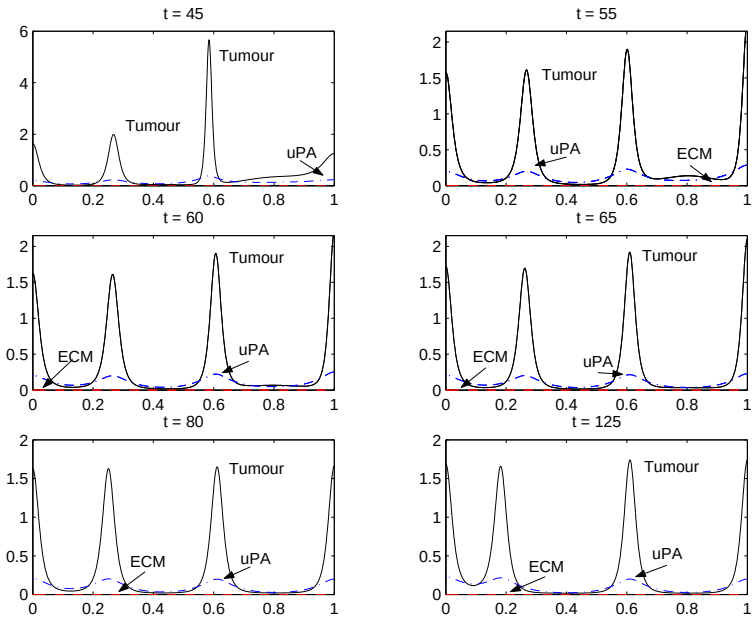

FIGURE 20. *Sequence of profiles showing the evolution of the tumour cell density $c(x,t)$ (solid black line), the protease concentration $u(x,t)$ (dot-dashed blue line) and the ECM density $v(x,t)$ (dashed red line), showing the effect of cycling proliferatinf rates. Parameter values:* $D_c = 10^{-3}, D_u = 10^{-3}, \chi_c = 0.03, \xi_c = 0.05, \alpha = 0.1, \beta = 0.3, \delta = 10, \mu_1 = 0.05, \mu_2 = 0.1, L = 0.1cm, \tau = 10^4 sec.$

a continuous band of cancer cell density. It is worth noting that in Figure 17, and considering the same time that we mention describing Figure 21, we observe two clusters of static cancer cells in a dormant state.

6. **Discussion.** In this paper we have presented a basic, minimal mathematical model of cancer cell invasion of tissue and investigated the effect of chemotaxis, haptotaxis as well as proliferation. In this regard, the model focuses specifically on the role of the urokinase plasminogen activation system in cancer cell invasion of tissue. The main achievement of this model is to demonstrate that fairly simple mathematical models representing the interactions of the components of the plasminogen activation system coupled with cell migration were able to capture the main characteristic effects of the system in cancer progression and invasion. The results of the simulations of the model show a very rich dynamic spatio-temporal behaviour. The observed spatio-temporal heterogeneities in the solution profiles arise from the complex interplay between proliferative effects - cancer cell proliferation and matrix remodelling - and gradient-driven migration (chemotaxis and haptotaxis). Cancer cells initially degrade the matrix through the uPA system and can initially move via taxis into the degraded matrix, coupled with cell proliferation. However, as the matrix remodels, this provides the cancer cells with the opportunity to "re-degrade" this re-generated matrix with the consequence that multiple clusters of invading cancer cells appear throughout the domain.

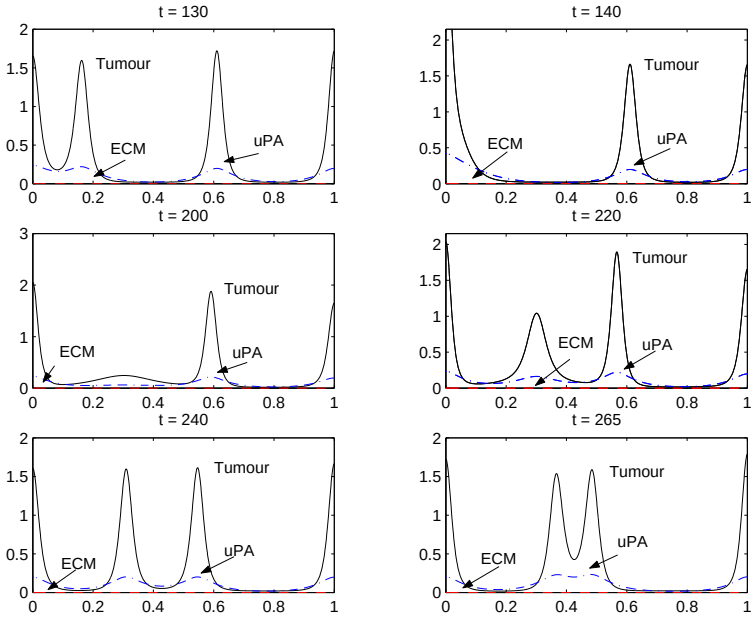

FIGURE 21. *Sequence of profiles showing the evolution of the tumour cell density $c(x,t)$ (solid black line), the protease concentration $u(x,t)$ (dot-dashed blue line) and the ECM density $v(x,t)$ (dashed red line), showing the effect of cycling proliferatinf rates. Parameter values:* $D_c = 10^{-3}, D_u = 10^{-3}, \chi_c = 0.03, \xi_c = 0.05, \alpha = 0.1, \beta = 0.3, \delta = 10, \mu_1 = 0.05, \mu_2 = 0.1, L = 0.1cm, \tau = 10^4 sec.$

The haptotaxis-only model results demonstrate the impact of interactions between tumour cells and the tisuue components on possible metastasis. Therefore, we observe that by increasing the haptotactic coefficient ξ_c, a large cluster of cancer cells breaks away from the primary tumour and migrates into the region. However, by the time that this secondary tumour reaches the boundary, it reverses its direction driven by the gradient of the undegraded extracellular components. We could presume that our boundary represents a hard tissue or bone and therefore we could assume biologically that the cancer cells were unable to penetrate the hard tissue or bone and thus reverse their direction directed by ECM components gradient.

The addition of the cancer cell proliferation term and tissue remodelling term affected only the speed of the invasion since once again the invasion was successful. However, when we consider the proliferation of the cancer cells as a result of uPA-bound cell-surface receptor signalling we note the break-off of a large cluster of cells. It is important also to mention that when cells move via random migration and haptotaxis and the intensity of the random movement is dependent upon extracellular matrix components *i.e.* vitronectin, then a large cluster of cancer cells breaks away from the primary tumour. Therefore, we could assume that a combined anti-protease therapy accompanied by a haptotactic - anti-adhesive blocking agent may result in faster cancer remission and could prevent any early increase in invasion.

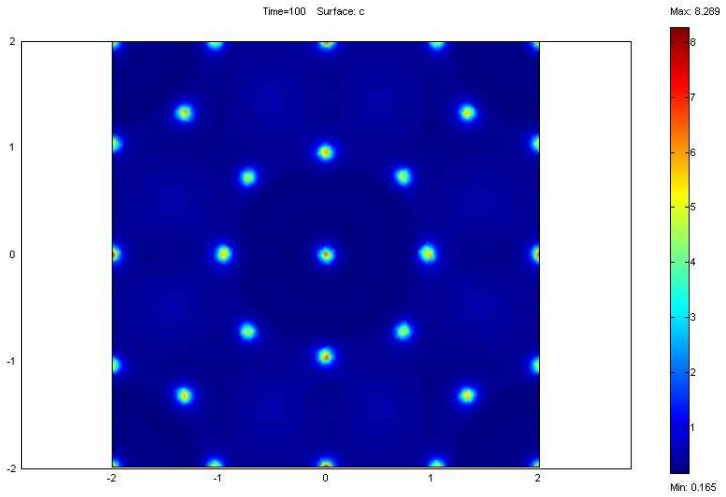

FIGURE 22. *Cancer cell density profile from a numerical computation of the 2-dimensional model (15). Plot shows the heterogeneous distribution of cancer cell density as it invades the tissue.*

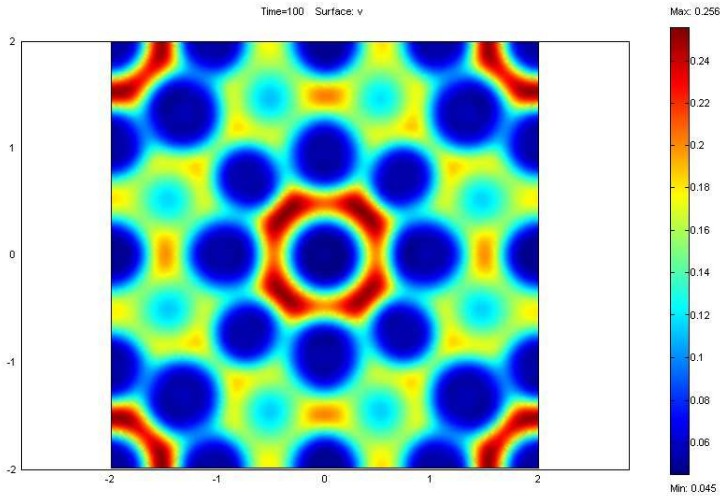

FIGURE 23. *Extracellular matrix (tissue) density profile from a numerical computation of the 2-dimensional model (15). Plot shows the heterogeneous distribution of tissue density as it is invaded by the cancer cells.*

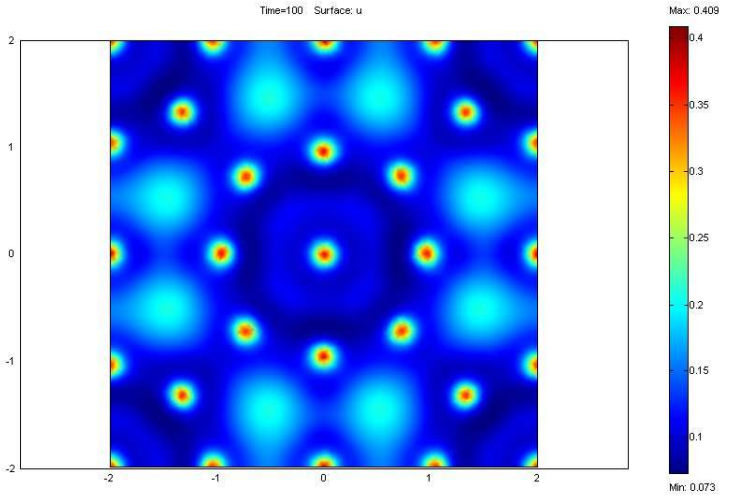

FIGURE 24. *uPA concentration profile from a numerical computation of the 2-dimensional model (15).*

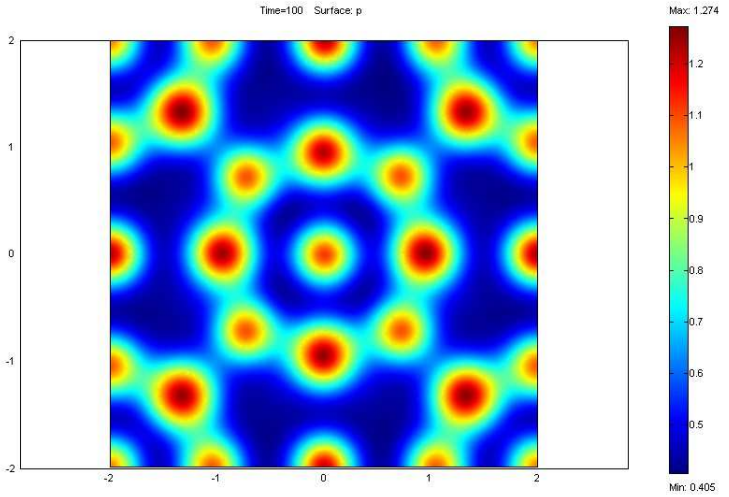

FIGURE 25. *PAI-1 concentration profile from a numerical computation of the 2-dimensional model (15).*

The results of the model have shown that the spatially heterogeneous distributions of cancer cells which arise as a consequence of simple binding reactions and gradient-driven migration may help to explain certain clinically and experimentally observed phenomena in carcinoma and multicellular spheroids, *i.e.* the

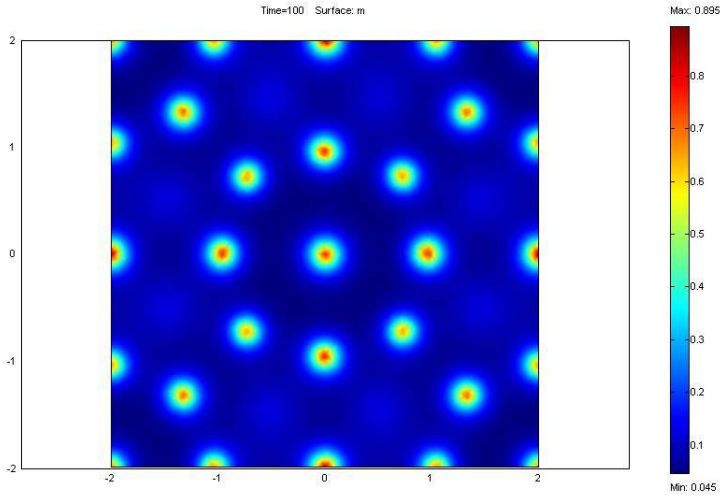

FIGURE 26. *Plasmin concentration profile from a numerical computation of the 2-dimensional model (15).*

heterogeneous "anarchic" spatial distribution of proliferating cancer cells and tissue. Undoubtedly, the urokinase plasminogen activation system is far more complex than the simplified approach outlined above ([59]). In this regard, the specific functions of plasminogen activator inhibitor-1 (PAI-1) and plasmin should be included explicitly for a more accurate reflection of the underlying biology since these are likely to influence tissue invasion as well. In this regard, the work of Chaplain and Lolas ([23]) has started to pursue this line of investigation and developed a model of cancer cell invasion including both plasminogen activator inhbitor-1 (PAI-1) as a uPA (protease) inhibitor and vitronectin (haptotactic blocking agent) ligand, as well as plasmin activation. The system considered there is as follows:

$$
\begin{aligned}
\frac{\partial c}{\partial t} &= \underbrace{D_c \frac{\partial^2 c}{\partial x^2}}_{Random\,Motion} - \frac{\partial}{\partial x}\Big(\underbrace{\chi_c c \frac{\partial u}{\partial x}}_{\text{uPA}-\text{chemo}} + \underbrace{\zeta_c c \frac{\partial p}{\partial x}}_{\text{PAI}-1-\text{chemo}} + \underbrace{\xi_c c \frac{\partial v}{\partial x}}_{\text{VN}-\text{hapto}} \Big) + \\
&\quad \underbrace{\phi_{13}\, c\, u}_{proliferation} + \underbrace{\mu_1\, c\,(1-c)}_{proliferation}, \\
\frac{\partial v}{\partial t} &= \underbrace{-\delta\, v\, m}_{degradation} + \underbrace{\phi_{21}\, u\, p}_{uPA/PAI-1} - \underbrace{\phi_{22}\, v\, p}_{PAI-1/VN} + \underbrace{\mu_2\, v\,(1-v)}_{proliferation}, \\
\frac{\partial u}{\partial t} &= \underbrace{D_u \frac{\partial^2 u}{\partial x^2}}_{Diffusion} - \underbrace{\phi_{31}\, p\, u}_{\text{PAI}-1/\text{uPA}} - \underbrace{\phi_{33}\, c\, u}_{\text{uPA/cells}} + \underbrace{\alpha_{31}\, c}_{production}\ ,
\end{aligned}
\tag{15}
$$

$$\frac{\partial p}{\partial t} = \underbrace{D_p \frac{\partial^2 p}{\partial x^2}}_{Diffusion} - \underbrace{\phi_{41}\, p\, u}_{\text{PAI}-1/\text{uPA}} - \underbrace{\phi_{42}\, p\, v}_{\text{PAI}-1/\text{VN}} + \underbrace{\alpha_{41}\, m}_{production}$$

$$\frac{\partial m}{\partial t} = \underbrace{D_m \frac{\partial^2 m}{\partial x^2}}_{Diffusion} - \underbrace{\phi_{51}\, p\, u}_{\text{PAI}-1/\text{uPA}} + \underbrace{\phi_{52}\, p\, v}_{\text{PAI}-1/\text{VN}} + \underbrace{\phi_{53}\, u\, c}_{\text{uPA/cells}} .$$

where p and m represent the concentrations of plasminogen activator inhibitor (PAI-1) and plasmin respectively. The computational simulations carried out in this paper demonstrated even richer heterogeneous spatio-temporal dynamics caused by a "taxis-driven-instability" of the underlying spatially homogeneous steady-state (cf. Turing patterns). This work has recently been extended to 2-dimensions and pictures showing the profiles of the variables in the above model are shown in figures (22)-(26).

Acknowledgments. MAJC gratefully acknowledges support from the EU Marie Curie Research Training Network Grant *"Modelling, Mathematical Methods and Computer Simulations of Tumour Growth and Therapy"*, contract number MRTN-CT-2004-503661.

REFERENCES

[1] Aguirre Ghiso J.A., Alonso D.F., Farías E.F., Gomez D.E. and and Bal De Kier Joffè E.,Deregulation of the signaling pathways controlling urokinase production. Its relationship with the invasive phenotype, *European Journal of Biochemistry*, 263 (1999), 295–304.

[2] Alberts B., Bray D., Lewis J., Raff M., Roberts K., Watson J.D., Molecular Biology of the Cell, Garland Publishing (1994).

[3] Alitalo K., Tammela T. and Petrova T.V., Lymphangiogenesis in development and human disease, *Nature*, 438 (2005), 946–953.

[4] Anderson A.R.A. and Chaplain M.A.J., Newman E.L., Steele R.J.C., and Thompson A.M., Mathematical modelling of tumour invasion and metastasis, *Journal of Theoretical Medicine*, 2 (2000), 129 –154.

[5] Anderson A.R.A., A hybrid mathematical model of solid tumour invasion: The importance of cell adhesion, *Mathematical Medicine and Biology*, (2) 22 (2005), 163–186.

[6] Andreasen P.A., Kjøller L., Christensen L. and Duffy M.J., The urokinase-type plasminogen activator system in cancer metastasis: A review, *International Journal of Cancer*, 72 (1997), 1–22.

[7] Andreasen P.A., Egelund R. and Petersen H.H., The plasminogen activation system in tumor growth, invasion, and metastasis, *Cellular and Molecular Life Sciences*, 57 (2000), 25–40.

[8] Atkins P.W., Physical Chemistry 3rd edition, Oxford University Press (1989).

[9] Aznavoorian S., Stracke M.L., Krutzsch H., Schiffmann E. and Liotta L.A., Signal transduction for chemotaxis and haptotaxis by matrix molecules in tumor cells, *The Journal of Cell Biology*, 110 (1990), 1427–1438.

[10] Aznavoorian S., Murphy A.N., Stetler-Stevenson W.G. and Liotta L.A., Molecular aspects of tumor cell invasion and metastasis, *Cancer*, 71 (1993), 1368–1383.

[11] Bajpai A., and Baker J.B., Cryptic urokinase binding sites on human foreskin fibroblasts, *Biochemical and Biophysical Research Communications*, 133 (1985), 475–482.

[12] Besser D., Verde P., Nagamine Y., and Blasi F., Signal transduction and the u-PA/u-PAR system, *Fibrinolysis*, 10 (1996), 215–237.

[13] Blasi F., Vassalli J-D., and Danø K., Urokinase-type plasminogen activator: Proenzyme, receptor, and inhibitors, *Journal of Cell Biology*, 104 (1987), 801–804.

[14] Bray D., Cell Movements: From molecules to motility, Garland Publishing (2000).

[15] Busso N., Masur S.K., Lazega D., Waxman S., and Ossowski L., Induction of cell migration by pro-urokinase binding to its receptor: possible mechanism for signal-transduction in human epithelial cells, *Journal of Cell Biology*, 126 (1994), 259–270.

[16] Byrne H.M., Chaplain M.A.J., Pettet G.J., and McElwain D.L.S., A mathematical model of trophoblast invasion, *Journal of Theoretical Medicine*, 1 (1998), 275–286.
[17] Carter S.B., Haptotaxis and the mechanism of cell motility, *Nature*, 213 (1967), 256–260.
[18] Chambers A.F., and Matrisian L.M., Changing views of the role of matrix metalloproteinases in metastasis, *Journal of the National Cancer Institute*, 89 (1997), 1260–1270.
[19] Chambers A.F., Groom A.C., and MacDonald I.C., Dissemination and growth of cancer cells in metastatic sites, *Nature Revies*, 2 (2002), 563–572.
[20] Chaplain M.A.J. and Stuart A.M., A mathematical model for the diffusion of tumour angiogenesis factor into the surrounding host tissue, *IMA Journal of Mathematics Applied in Medicine & Biology*, 8 (1991), 191–220.
[21] Chaplain M.A.J., The mathematical modelling of tumour angiogenesis and invasion, *Acta Biotheoretica*, 43 (1995), 387–402.
[22] Chaplain M.A.J., and Anderson A.R.A., Mathematical modelling, simulation and prediction of tumour-induced angiogenesis, *Invasion & Metastasis*, 16 (1996), 222–234.
[23] Chaplain M.A.J. and Lolas, G., Mathematical modelling of cancer cell invasion of tissue: The role of the urokinase plasminogen activation system, *Mathematical Models and Methods in Applied Sciences*, 15 (2005), 1685–1734.
[24] Chapman H.A., Plasminogen activators, integrins, and the coordinated regulation of cell adhesion and migration, *Current Opinion in Cell Biology*, 9 (1997), 714–724.
[25] Collen D., Zamarron C., Lijnen H.R., and Hoylaerts M., Activation of plasminogen by prourokinase, *Journal of Biological Chemistry*, 261, 1259–1266, (1986).
[26] Comper W.D., Extracellular Matrix Volume 2 Molecular Components and Interactions, Harwood Academic Publishers (1996).
[27] Conese M., and Blasi F., The urokinase/urokinase-receptor system and cancer-invasion, *Baillière's Clinical Haematology*, 8 (1995), 365–389.
[28] Conese M., Blasi F., Urokinase/urokinase receptor system: Internalization/degradation of urokinase-serpin complexes. Mechanism and regulation, *Biological Chemistry Hoppe-Seyler*, 376 (1995), 143–155.
[29] Curtis A.S.G., The measurement of cell adhesiveness by an absolute method, *Journal of Embryology and Experimental Morphology,* 22 (1969), 305–325.
[30] Czekay R-P., Aertgeerts K., Curriden S.A., and Loskutoff D.J., Plasminogen activator inhibitor-1 detaches cells from extracellular matrices by inactivating integrins, *Journal of Cell Biology*, (5) 160 (2003) 781–791.
[31] Danø K., Anderson P.A., Grondahl-Hansen J., Kristensen P., Nielsen L.S. and Skriver L., Plasminogen activators, tissue degradation and cancer, *Advanced Cancer Research*, 44 (1985), 139–266.
[32] Danø K., Behrendt N., Brunner N., Ellis V., Ploug M. and Pyke C., The urokinase receptor. Protein structure and role in plasminogen activation and cancer invasion, *Fibrinolysis*, 8 (1994), 189–203.
[33] Danø K., Behrendt N., Høyer-Hansen G., Johnsen M., Lund L.R., Ploug M. and Rømer J., Plasminogen activation and cancer, *Thrombosis and Haemostasis*, 93 (2005), 676–681.
[34] Deng G., Curriden S.A., Wang S., Rosenberg S., Loskutoff D.J., Is plasminogen activator inhibitor-1 the molecular switch that governs urokinase receptor-mediated cell adhesion and release ? *Journal of Cell Biology*, 134 (1996), 1563–1571.
[35] uffy M.J., Urokinase plasminogen activator: A prognostic marker in multiple types of cancer, *Journal of Surgical Oncology*, 71 (1999), 130–135.
[36] Edelstein-Keshet L., *Mathematical Models in Biology*, McGraw-Hill, Inc (1988).
[37] Estreicher A., Mühlhauser, Carpentier J-L., Orci L., and Vassali J-D. , The receptor for urokinase type plasminogen activator polarizes expression of the protease to the leading edge of migrating monocytes and promotes degradation of enzyme inhibitor complexes, *Journal of Cell Biology*, 111 (1990), 783–792.
[38] Fazioli F., Resnati M., Sidenius N., Higashimoto Y., Appella E., and Blasi F., A urokinase-sensitive region of the human urokinase receptor is responsible for its chemotactic activity, *The EMBO Journal*, 16 (1997), 7279–7286.
[39] Fidler I.J., The biology of cancer metastasis or, "you cannot fix it if you do not know how it works", *Bioessays*, 13 (1991), 551–554.
[40] Fidler I.J., The pathogenesis of cancer metastasis: the 'seed and soil' hypothesis revisited, *Nature Reviews*, 3 (2002), 1–6.
[41] Folkman J., Tumour angiogenesis, *Advances in Cancer Research*, 19 (1974), 331–358.

[42] Folkman J., The vascularization of tumours, *Scientific American*, 234 (1976), 58–73.
[43] Fox S.B, Taylor M., Grøndahl-Hansen J., Kakolyris S., Gatter K.C., and Harris A.L., Plasminogen activator inhibitor-1 as a measure of vascular remodelling in breast cancer, *Journal of Pathology*, 195 (2001), 236–243.
[44] Gatenby R.A., and Gawlinski, E.T., A reaction-diffusion model of cancer invasion, *Cancer Research*, 56 (1996), 5745–5753.
[45] Gyetko M.R., Todd R.F.,III, Wilkinson C.C., and Sitrin R.G., The urokinase receptor is required for human monocyte chemotaxis in vitro, *Journal of Clinical Investigation*, 93 (1994), 1380–1387.
[46] Hanahan D., and Weinberg R.A., The hallmarks of cancer, *Cell*, 100 (2000), 57–70.
[47] Irigoyen J.P., Muñoz-Cánoves P., Montero L., Koziczak M., and Nagamine Y., The plasminogen activator system: biology and regulation, *Cellular and Molecular Life Sciences*, 56 (1999), 104–132.
[48] Kanse S.M., Kost C., Wilhelm O.G., Andreasen P.A., and Preissner K.T., The urokinase receptor is a major vitronectin-binding protein on endothelial cells, *Experimental Cell Research*, 224 (1996), 344–353.
[49] Kjøller L., Kanse S.M., Kirkegaard T., Rodenburg K.W., Rønne E., Goodmann S.L., Preissner K.T., Ossowski L., and Andreasen P.A., Plasminogen activator inhibitor-1 represses integrin- and vitronectin-mediated cell migration independently of its function as an inhibitor of plasminogen activation, *Experimental Cell Research*, 232 (1997), 420–429.
[50] Kjøller L., The urokinase plasminogen activator receptor in the regulation of the actin cytoskeleton and cell motility, *Biological Chemistry*, 383 (2002), 5–19.
[51] Kohn E.C., and Liotta L.A., Molecular insights into cancer invasion: strategies for prevention and intervention, *Cancer Research*, 51, 1856–1862, (1995).
[52] Lachowicz, M., Micro and meso scales of description corresponding to a model of tissue invasion by solid tumours, *Mathematical Models and Methods in Applied Sciences*, 11 (2005), 1667–1683.
[53] Lackie, J.M. and Wilkinson, P.C. (Eds.), Biology of the Chemotactic Response, Cambridge University Press, Cambridge (1981).
[54] Lauffenburger D., A simple model for the effects of receptor-mediated cell-substratum adhesion on cell migration, *Chemical Engineering Science*, 44 (1989), 1903–1914.
[55] Lauffenburger D.A. and Horwitz A.F., Cell migration: A physically integrated molecular process, *Cell*, 84 (1996), 359–369.
[56] Liotta L.A., Tumour invasion and metastases: role of the extracellular matrix, *Cancer Research*, 46 (1986), 1–7.
[57] Liotta L.A., and Stetler-Stevenson W.G., Tumor invasion and metastasis as targets for cancer therapy, *Cancer Research*, 51 (1991), 5054–5059.
[58] Liotta L.A., and Clair T., Checkpoint for invasion, *Nature*, 405 (2000), 287–288.
[59] Lolas, G., Mathematical modelling of the urokinase plasminogen activation system and its role in cancer invasion of tissue, PhD Thesis, University of Dundee (2003).
[60] Mantzaris, N.V., Webb, S. and Othmer, H.G., Mathematical modelling of tumour-induced angiogenesis, 49 (2004), 111–187.
[61] Mignatti P. and Rifkin D.B., Biology and biochemistry of proteinases in tumor invasion, *Physiological Reviews*, 73 (1993), 161–195.
[62] Murray J.D., *Mathematical Biology: Spatial Models and Biomedical Applications*, Spinger-Verlag (2003).
[63] Naski M.C., Lawrence D.A., Mosher D.F., Podor T.J., and Ginsburg D., Kinetics of inactivation of α-thrombin by plasminogen activator inhibitor-1, *Journal of Biological Chemistry*, 268, 12367–12372, (1993).
[64] Nguyen D.H.D., Hussaini I.M., and Gonias S.L., Binding of urokinase-type plasminogen activator to its receptor in MCF-7 cells activates extracellular signal-regulated kinase 1 and 2 which is required for increased cellular motility, *The Journal of Biological Chemistry*, 273 (1998), 8502–8507.
[65] Nykjær A., Conese M., Christensen E.I., Olson D., Cremona O., Gliemann J. and Blasi F., Recycling of the urokinase receptor upon internalization of the uPA: serpin complexes, *The EMBO Journal*, 16 (1997), 2610–2620.
[66] Orme M.E. and Chaplain M.A.J., A mathematical model of vascular tumour growth and invasion, *Mathematical and Computer Modelling,* 23 (1996), 43–60.

[67] Pepper M.S., Sappino A.-P., Stöcklin R., Montesano R., Orci L., and Vassalli J.-D., Upregulation of urokinase receptor expression on migrating endothelial cells, *The Journal of Cell Biology*, 122 (1993), 673–684.
[68] Pepper M.S., Role of the matrix metalloproteinase and plasminogen activator-plasmin systems in angiogenesis, *Arteriosclerosis, Thrombosis and Vascular Biology*, 21 (2001a), 1104–1117.
[69] Perumpanani A.J., Sherratt J.A., Norbury J., Byrne H.M., Biological inferences from a mathematical model for malignant invasion, *Invasion & Metastasis*, 16 (1996), 209–221.
[70] Perumpanani A.J., Simmons D.L., Gearing A.J.H., Miller K.M., Ward G., Norbury J., Schneemann M., and Sherratt J.A., Extracellular matrix-mediated chemotaxis can impede cell migration, *Proceedings of the Royal Society of London, Series B*, 265 (1998), 2347–2352.
[71] Plesner T., Behrendt N., and Ploug M., Structure, function and expression on blood and bone marrow cells of the urokinase-type plasminogen activator receptor, uPAR, *STEM Cells*, 15 (1997), 398–408.
[72] Preziosi, L. (Ed.), *Cancer Modelling and Simulation*, Chapman & Hall/CRC Press (2003).
[73] Rakic J.M., Maillard C., Jost, M., Bajou K., Masson V., Devy L., Lambert V., Foidart J.M., and Noël A., Role of plasminogen activator-plasmin system in tumor angiogenesis, *Cellular and Molecular Life Sciences*, 60, 463–473, (2003).
[74] Resnati M., Guttinger M., Valcamonica S., Sidenius N, Blasi F., and Fazioli F., Proteolytic cleavage of the urokinase receptor substitutes for the agonist-induced chemotactic effect, *EMBO Journal*, 9 (1996), 467–470.
[75] Sherratt J.A., and Murray J.D., Models of epidermal wound healing, *Proceedings of the Royal Society of London Series B,* 241 (1990), 29–36.
[76] Sherratt J.A., Chemotaxis and chemokinesis in eukaryotic cells: The Keller-Segel equations as an approximation to a detailed model, *Bulletin of Mathematical Biology*, 56 (1994), 129–146.
[77] Stokes C.L., Lauffenburger D.A., and Williams S.K., Migration of individual microvessel endothelial cells: stochastic model and parameter measurement, *Journal of Cell Science*, 99 (1991), 419–430.
[78] Stokes C.L., and Lauffenburger D., Analysis of the roles of microvessel endothelial cell random motility and chemotaxis in angiogenesis, *Journal of Theoretical Biology*, 152 (1991), 377–403.
[79] Stoppelli M.P., Corti A. Soffientini A., Cassani G., Blasi F., and Assoian R.K., Differentiation-enhanced binding of the amino-terminal fragment of human urokinase plasminogen activator to a specific receptor on U937 monocytes, *Proceedings of the National Academy of Sciences USA*, 82 (1985), 4939–4943.
[80] Tarui T., Mazar A.P., Cines D.B., and Takada Y., Urokinase-type plasminogen activator receptor (CD87) is a ligand for integrins and mediates cell-cell interaction, *The Journal of Biological Chemistry*, 276 (2001), 3983–3990.
[81] Waltz D.A. and Chapman H.A., Reversible cellular adhesion to vitronectin linked to urokinase receptor occupancy, *Journal of Biological Chemistry*, 269 (1994), 14746–14750.
[82] Waltz D.A, Natkin L.R., Fujita R.M., Wei Y., and Chapman H.A., Plasmin and plasminogen activator inhibitor type 1 promote cellular motility by regulating the interaction between the urokinase receptor and vitronectin, *Journal of Clinical Investigation*, 100 (1997), 58–67.
[83] Wei Y., Waltz D.A., Rao N., Drummond R.J., Rosenberg S., and Chapman H.A., Identification of the urokinase receptor as an adhesion receptor for vitronectin, *The Journal of Biological Chemistry,* 269 (1994), 32380–32388.
[84] Yebra M., Goretzki L., Pfeifer M., and Mueller B.M., Urokinase-type plasminogen activator binding to its receptor stimulates tumor cell migration by enhancing integrin-mediated signal transduction, *Experimental Cell Research*, 250 (1999), 231–240.
[85] Yu, W., Kim, J. and Ossowski, L., Reduction in surface urokinase receptor forces malignant cells into a protracted state of dormancy, *Journal of Cell Biology*, 137 (1997), 767–777.

Received February 2006; revised June 2006.

E-mail address: chaplain@maths.dundee.ac.uk
E-mail address: georgioslolas@gmail.com